Article

On the Link between Plastic Wake Induced Crack Closure and the Fatigue Threshold

Rhys Jones [1,2,*] , Andrew Ang [1] , Nam D. Phan [3] and Michael Nicholas [4]

1   ARC Industrial Transformation Training Centre on Surface Engineering for Advanced Materials, Faculty of Science, Engineering and Technology, Swinburne University of Technology, John Street, Hawthorn, VIC 3122, Australia; aang@swin.edu.au
2   Centre of Expertise for Structural Mechanics, Department of Mechanical and Aerospace Engineering, Monash University, Clayton, VIC 3800, Australia
3   Structures Division, Naval Air Systems Command, Patuxent River, MD 20670, USA
4   US Army Research Laboratory, U.S. Army Combat Capabilities Development Command Weapons and Materials Research Directorate, Aberdeen Proving Ground, Aberdeen, MD 21005, USA; michael.b.nicholas3.civ@army.mi
*   Correspondence: rhys.jones@monash.edu

Abstract: This purpose of this paper is to examine the relationship between crack growth equations based on Elber's original plastic wake induced crack closure concept and the fatigue threshold as defined by the American Society for Testing and Materials (ASTM) fatigue test standard ASTM E647-15el. It is shown that, for a number of conventionally manufactured metals, the function $U(R)$, where R is the ratio of the minimum to maximum applied remote stress, that is used to relate the stress intensity factor ΔK to the effective stress intensity factor ΔK_{eff} is inversely proportional to the fatigue threshold $\Delta K_{th}(R)$. This finding also results in a simple closed form equation that relates the crack opening stress intensity factor $K_o(R)$ to ΔK, K_{max}, and the fatigue threshold terms $\Delta K_{th}(R)$ and $\Delta K_{eff,th}$. It is also shown that plotting da/dN as function of $\Delta K/\Delta K_{th}(R)$ would appear to have the potential to help to identify the key fracture mechanics parameters that characterise the effect of test temperature on crack growth. As such, for conventionally manufactured metals, plotting da/dN as function of $\Delta K/\Delta K_{th}(R)$ would appear to be a useful addition to the tools available to assess the fracture mechanics parameters affecting crack growth.

Keywords: fatigue crack growth; crack closure; fatigue threshold; additive manufacturing; temperature effects

1. Introduction

Whilst this paper focuses on fracture mechanics based tools for assessing crack growth in aerospace structures, it should be noted that the study of crack growth is central to a wide crossection of industries, viz: rail, nuclear power, offshore oil and gas, etc. Indeed, to put things into perspective, ref. [1] states that "in the United States of America (USA), there are more trips per day over structurally deficient bridges than there are McDonald's hamburgers eaten in the entire USA".

The certification requiremets for military aircraft are delineated in MIL-STD-1530D [2]. The guidelines for the airworthiness certification of additively manufactured (AM) and cold spray additively manufactured (CSAM) parts are gven in United Stes Air Force Structures Bulletin EZ-SB-19-01 [3]. Both MIL-STD-1530D and EZ-SB-19-01 mandate that all durability and damage tolerance (DADT) analyses be performed using linear elastic fracture mechanics (LEFM). Indeed, EZ-SB-19-01 stated that the accurate prediction of the DADT of an AM part is perhaps the greatest challenge facting the airworthiness acceptance of AM parts. Consequently, in this paper, we will confine our focus on fatigue crack growth studies that relate da/dN to ΔK. Here a is the crack length, N is the number of fatigue cycles,

and $\Delta K = K_{max} - K_{min}$, where K_{max} and K_{min} are the maximum and minimum values of the crack tip stress intensity factor (K) in a load cycle.

As a result, the DADT assessment of conventionall manufactured, AM and CSAM parts must be based on the appropriate da/dN versus ΔK curve. However, it is now known [4–20] that the variability in the da/dN versus ΔK curves associated with the growth of long cracks in more than one hundred and twenty independent tests performed on a range of additively manufactured (AM) materialscan often be accounted for by expressing the crack growth rate (da/dN) as a function of $\Delta\kappa$, where $\Delta\kappa$ is the Schwalbe crack driving force [21], and by allowing for the effect of the manufacturing process on just two parameters, namely the cyclic fatigue threshold and the fracture toughness. Here $\Delta\kappa$ is Schwalbe's crack driving force which is defined as:

$$\Delta\kappa = (\Delta K - \Delta K_{thr})/\sqrt{(1 - K_{max}/A)} \tag{1}$$

The terms ΔK_{thr} and A in Equation (1) are the fatigue threshold and the apparent cyclic fracture toughness respectively. The additively manufactured materials for which this observation has been found to hold include: Ti-6Al-4V [6,7,11,12], Inconel 718 [5], Inconel 625 [5], 316L steel [6,17,20], 304L steel [20], Aermet 100 steel [6], 17-4 Ph steel [15], Scalmalloy [12], an aluminium-scandium-magnesium alloy [4], 18Ni 250 Maraging steel [8,19]. This observation also appears to hold for a range of conventionally manufactured materials [22–29], a range of CSAM materials [20] and for plasma sprayed metals and alloys [30].

Figure 5 can often be predicted by setting the fatigue threshold term in Equation (1) to a small value, typically in the range $0.1 \leq \Delta K_{thr} \leq 0.3$ MPa $\sqrt{\text{m}}$.

(i) The multi-axial fatigue life of AM parts can often be computed using the same formulation [13,18];
(ii) The variability in the growth of long cracks in conventionally manufactured metals can also often be captured by allowing for the variability associated with the fatigue threshold [22].

Indeed, variants of this approach have also been shown to be able to model delamination growth in composites as well as cohesive crack growth in adhesives and nanocomposites, see [31–37].

Many legacy fixed and rotary wing aircraft make extensive use of 7000 and/or 2000 series aluminium alloys. Consequently, the recent finding [38] that Boeing Intelligence and Weapon Systems laser powder bed fusion (LPBF) Scalmalloy has a damage tolerance that is superior to that of the conventionally manufactured aluminium alloy 7075-T6 has highlighted the potential of Scalmalloy to be used to print limited life load bearing parts. However, as previously noted USAF Structures Bulletin EZ-19-01 [3] states that the accurate prediction of its durability and damage tolerance (DADT) is one of the most challenging issues facing the acceptance of AM parts. These various findings/observations raise the question: Can we link the observations delineated above, namely that the fatigue threshold would appear to be a key parameter in characterising crack growth in AM materials and cold spray repairs, to the crack closure concept that is commonly used to assess the damage tolerance of conventionally built aerospace parts?

In this context it should be noted that Paris et al. [39] were the first to suggest that, since [40,41] had shown that the stress-intensity factor K, uniquely characterises the near tip stress field, then the rate of fatigue crack growth should be a function of ΔK and K_{max} [39,42,43]. However, when expressing da/dN as a function of ΔK it is found that the resultant da/dN versus ΔK curves can become dependent on the R ratio. (Here R is defined as $R = K_{min}/K_{max}$.)

Frost [44] subsequently revealed, for long cracks, the existence of a fatigue threshold ($\Delta K_{th}(R)$), which can be a function of the R ratio, below which a crack will not grow. (The ASTM fatigue test standard ASTM E647-15el [45] defines ΔK_{th} as the value of ΔK_{th} at a crack growth rate da/dN of 10^{-10} m/cycle.) Elber [46,47] subsequently introduced the idea that the R ratio dependency of the da/dN versus ΔK curves could be accounted for

by introducing what was termed an "effective stress intensity factor" (ΔK_{eff}) that accounts for plastic wake induced crack closure. (Here it should be noted that, as a result of the stress singularity at a crack tip the linear elastic fracture mechanics solution suggests that the region surrounding the crack will see an infinite stress. In reality, this region will yield. As a result, during fatigue crack growth the crack will grow through this yielded material and in the process the material is unloaded. This process results in compressive stresses behind the crack and the possibility that the crack faces will close. It is this process that is commonly refered to as "plastic wake induced crack closure. At this point, it should be mentioned that, whilst, as discussed in [48–53], there are other forms of crack closure and other formulations that attempt to account for this effect, this paper only addresses Elber's [46,47] original formulation and not the larger cross-section of formulations that are summarised in [52].

As outlined in [48–64] variants of this approach are now widely used to model the growth of long cracks in conventionally manufactured metals. However, it should also be noted that it has recently been suggested [65] that *R* ratio effects on the growth of long cracks can be interpreted as a reflection of the effect of the environment on the crack tip region rather than crack closure per se.

The literature also contains a number of other crack growth equations that are based on the hypothesis that da/dN should be a function of how much ΔK exceeds its threshold value [4,21,66–80]. As such the purpose of the present paper is to attempt to investigate a possible relationship between ΔK_{eff}, as originally defined by Elber [46,47], and the fatigue threshold term ΔK_{th}. This would provide a link between crack growth equations that are based on Elber's plastic wake induced crack closure concept and those that are based on the assumption that the crack growth rate should be a function of how much ΔK exceeds its threshold value.

It should be stressed that the findings presented in this paper do not constitute a proof that the effect of crack closure effects can always be interpreted as being reflected by its effect on the fatigue threshold. Indeed, this study is specifically confined to those materials where Elber's original formulation would appear to be a reasonable first approximation.

We also show that plotting da/dN as function of $\Delta K/\Delta K_{th}(R)$ would appear to have the potential to help identify the fracture mechanics parameters that characterise the effect of the test temperature on crack growth.

2. Materials and Methods

In order to achieve the goals stated above the authors have examined papers that are available in the open literature. Of the more than one hundred articles examined ninety eight are in peer reviewed Journals, five are available on the North American Space Administration (NASA) website, and one is available on the US Federal Aviation Administration (FAA) website. In those cases where the reference is not a Journal paper that is available in the open literature the web address of the reference is also given.

2.1. Choice of Materials

A focus of this paper is to examine if this phenomenon holds for a range of aerospace aluminium, steel, and titanium alloys. (By this we mean if plotting da/dN as a function of $\Delta K/\Delta K_{th}(R)$ collapses the various *R* ratio dependent da/dN versus ΔK curves onto a single master curve). In this context, it should be recalled that [81] had previously illustrated this phenomenon for a range of older aerospace aluminium alloys, namely 2024-T3, 7075-T651, 7050-T7451, 6013-T651 and 2324-T39. Consequently, we opted to study the more modern alloys 7085-T7452 [82], which is widely used on the F-35, and AA2524-T3 [83], which is a replacement for 2024-T3. On the other hand, given the role that [49,50] played in the development of the discipline, we thought it appropriate to examine if this phenomenon also held for the aluminium alloy 7055 that was studied in [49,50]. Similarly, crack growth in the aluminium alloy 7049 [84], which is widely used in military aircraft, is also examined. Furthermore, since [81] had not investigated stainless steels we opted to study 304L stainless

steel. Similarly, we chose to study the Titanium alloy Ti622 since it is being considered for the next generation of supersonic airliners [85].

In the case of the choice of an engine material there were two obvious choices, viz: Inconel 718 and Inconel 625. However, test data at both a range of *R* ratio's and temperatures was needed. As a result the super alloy GH4169 [86], which is the Chinese version of Inconel 718, was chosen.

Noting that, as previously mentioned, [81] revealed that in the case SLM Inconel 625 plotting *da/dN* as a function of $\Delta K / \Delta K_{th}(R)$ collapses the various *R* ratio dependent *da/dN* versus ΔK curves onto a single master curve, we opted to study a quite different AM material, namely Laser powder bed fusion (LPBF) built Hastelloy X [87]. (The SLM Inconel 625 sata analysed in [81] was taken from [88]).

The examples given [89,90], were chosen since they illustrated the temperature effects can sometimes merely reflect the effect of temperature on the fatigue threshold. In the case of [89] this example was chosen since it related to 304L stainless steel, which is widely used in aerospace. On the other hand [90] was chosen to investigate a quite different class of metals, namely medium entroy Cantor alloy CrCoNi.

2.2. The Relationship between Plasticity Induced Crack Closure and the Fatigue Threshold

Examining the above references revealed that Elber [46,47] was the first to introduce a function $U(R)$, which he [47] suggested was independent of both ΔK and K_{max}, that was used to define a term ΔK_{eff}, viz:

$$\Delta K_{eff} = U(R)\, \Delta K \tag{2}$$

such that, for long cracks that experience plastic wake induced crack closure, the resultant *da/dN* versus ΔK_{eff} curves associated with each individual *R* ratio dependent *da/dN* versus ΔK curve all fell onto a single curve regardless of the *R* ratio.

Several possible forms of this (scaling) function $U(R)$ are discussed in [50–56,59]. Here it should be noted that in [47] the function U was only a function of *R*. (A brief discussion of this statement is given in Appendix A) In such cases it thus follows from Equation (2) and from the facts that

(a) if as per Elber [47] $U(R)$ is only a function of *R* rather than of both ΔK and K_{max};
(b) and, if as per [47] for a given value of *R* the function $U(R)$ has a fixed (constant) value;

then if each *R* ratio dependent *da/dN* versus ΔK curve is to collapse onto a single *da/dN* versus ΔK_{eff} curve by merely multiplying (each value of) ΔK by the function $U(R)$, then Equation (2) can be rewritten in the form:

$$\Delta K_{eff} = (\Delta K_{eff,th} / \Delta K_{th}(R))\, \Delta K \tag{3}$$

Here $\Delta K_{eff,th}$ is the value of ΔK_{eff} at a crack growth rate *da/dN* of 10^{-10} m/cycle, and $\Delta K_{th}(R)$ is the value ΔK, for a given *R* ratio dependent crack growth curve, at a crack growth rate *da/dN* of 10^{-10} m/cycle respectively. A graphical explanation of this, for two arbitrary *R* ratios, which we have termed $R = R_1$ and $R = R_2$, is shown in Figure 1. (Equation (3) forces the various (scaled) *R* ratio dependent *da/dN* versus ΔK curves to coincide at a crack growth rate *da/dN* = 10^{-10} m/cycle). It thus follows that, for long cracks where crack growth is consistent with Elber's plastic wake induced crack closure equation, the function $U(R)$ can be expressed as:

$$U(R) = \Delta K_{eff,th} / \Delta K_{th}(R) \tag{4}$$

In other words ΔK_{eff}, as defined by Elber [46,47], should be linearly proportional to $\Delta K / \Delta K_{th}(R)$.
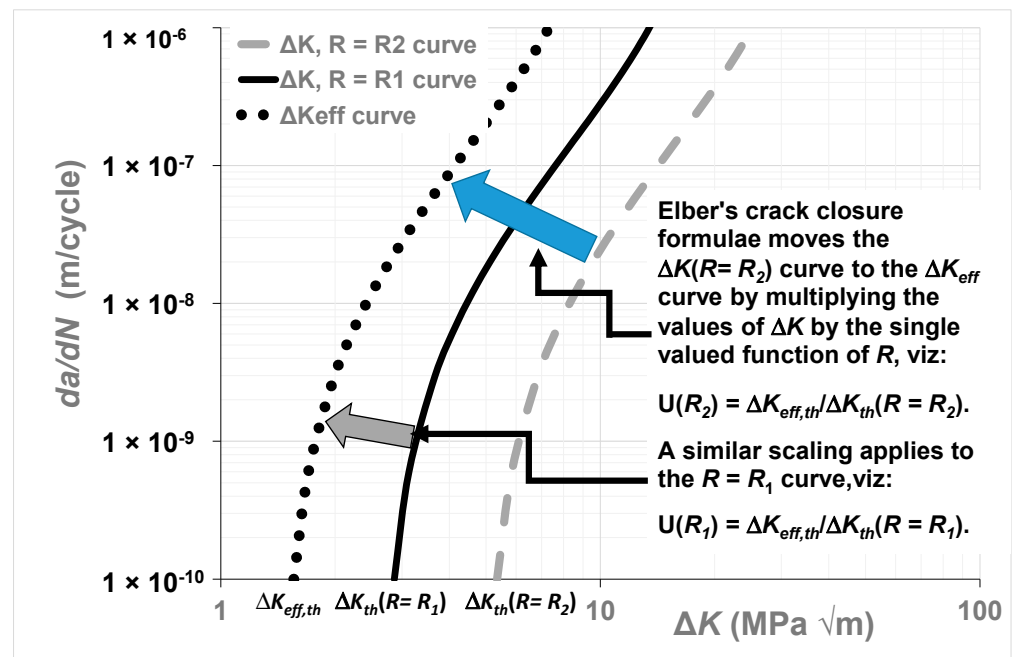
Figure 1. A graphical presentation of Elber's crack closure concept.

Elber [46,47] also introduced a function $K_o(R)$, which is a function of the *R*-ratio and which he defined as the value of the stress intensity factor at which a crack opens, such that

$$U(R) = (K_{max} - K_o(R))/(K_{max} - K_{min}) \tag{5}$$

As a result it is common to plot *da/dN* as a function of $(K_{max} - K_o(R))$. However, as explained in [49,50], it is sometimes best to plot *da/dN* as a function of $\Delta K_{2/\pi 0}$, where $\Delta K_{2/\pi 0} = (K_{max} - 2K_o(R)/\pi)$. This formulation, which [49–51] termed the $\Delta K_{2/\pi 0}$ approach, is discussed further in Appendix A.

Equations (4) and (5) enable us to determine a simple (closed form) equation that relates the crack opening stress intensity factor $K_o(R)$ to ΔK, K_{max} and $\Delta K_{th}(R)$, viz:

$$K_o(R) = K_{max} (1 - (1 - R) \Delta K_{eff,th} / \Delta K_{th}(R)) \tag{6}$$

which, when expressed in terms of the energy release rate *G* becomes

$$\sqrt{G_o}(R) = \sqrt{G}_{max} (1 - (1 - R) \Delta \sqrt{G_{eff,th}} / \Delta \sqrt{G_{th}}(R)) \tag{7}$$

It follows from the above discussion that whenever Elber's approach to plastic wake-induced crack closure, i.e., Equation (2), holds, then when *da/dN* is plotted against $\Delta K / \Delta K_{th}(R)$ the various "normalised" curves should also all fall onto a single curve. However, it is important to note that, as shown in [61,91–94], the use of the ASTM load-reducing test protocol to determine the fatigue crack thresholds can (sometimes) result in erroneous values of $\Delta K_{th}(R)$. Hence, Equation (4) may not (always) hold for data sets obtained using the American Society for Testing and Materials (ASTM) ASTM E647-15el [45] load-reducing test protocol, see Appendix B. As such, the use of the equation:

$$K_o(R) = K_{max} (1 - (1 - R) \Delta K'_{eff,th} / \Delta K'_{th}(R)) \tag{8}$$

where $\Delta K'_{eff,th}$ and $\Delta K'_{th}(R)$ are the values of ΔK_{eff} and $\Delta K(R)$ at a crack growth rate of *da/dN* = 10^{-8} m/cycle, may sometimes be more appropriate.

Furthermore, as illustrated in [95–97] there are a range of metals that whilst they have an *R* ratio dependency in the near threshold region, see minimal *R* ratio effects outside of this region and hence see little (if any) crack closure in the Paris region. As a result,

the concept of crack closure and the concept discussed in this paper does not hold for these materials.

Similarly, Appendix X3 (contained) in the fatigue test standard ASTM E647-15el [45] notes that it is not clear if a fatigue threshold exists for small naturally occurring cracks. This finding has significant implications when assessing the durability of metallic airframes since it means that the crack growth equation needed to assess the durability can differ from that associated with the closure free crack growth curve, see [19] for more details. A more detailed discussion on the state of the art can be found in [61,98,99].

To the best of the authors knowledge, the observation that, for long cracks, when da/dN was plotted against $\Delta K/\Delta K_{th}(R)$ the resultant R ratio dependent curves collapsed onto a single curve was first presented in [100]. This paper studied crack growth in: 17-4PH steam turbine blade steel tested in air at 90 °C at R ratio's that ranged from -1 to 0.9. A range of additional examples, viz: 7050-T7451, 20-23-T39, 2024-T3, 6013-T651, 7075-T6511, 7055-T6511, a cold-rolled metastable Austenitic stainless steel, and an additively manufactured Inconel 625 material built using selective laser melt (SLM) tested with the crack at different orientations to the build direction, were subsequently presented in [81].

An interesting, and possibly related, feature of [81] was that it was shown that for studies into delamination growth in double cantilever beam (DCB) composite laminates the da/dN versus $\Delta\sqrt{G}$ curves, where G is the energy release rate, were a strong function of the level of pre-cracking. However, when da/dN was plotted as a function of $\Delta\sqrt{G}/\Delta\sqrt{G}_{th}$ these different curves essentially collapsed onto a single curve. (The different da/dN versus $\Delta\sqrt{G}$ curves are as a result of the retardation due to the different levels of fibre bridging that are associated with the different levels of pre-cracking).

3. Illustrative Examples

To further illustrate this phenomenon, i.e., that when da/dN is plotted against $\Delta K/\Delta K_{th}(R)$ the resultant "normalised" curves can collapse onto a single curve, let us consider crack growth in the aluminium alloy AA7085-T7452 which is extensively used in the Lockheed F-35 Joint Strike Fighter (JSF). The $R = 0.1$ and 0.8 da/dN versus ΔK curves given in [82] for this material are reproduced in Figure 2. These curves were obtained from tests on specimens with an array of surface beaking defects, The corresponding da/dN versus $\Delta K/\Delta K_{th}$ curves are shown in Figure 3. Here we see that when normalised in this fashion the $R = 0.1$ and 0.8 da/dN versus $\Delta K/\Delta K_{th}$ curves do indeed collapse onto a single curve. The values of ΔK_{th} used in Figure 3 are given in Table 1.

To continue this study, let us next consider the $R = 0.1$ and 0.5 da/dN versus ΔK curves given in the NASA study [85] into crack growth in the titanium super alloy Ti-6A1-2Zr-2Cr-2Sn-2Mo (Ti-6-2-2-2-2). These da/dN versus ΔK curves, which were obtained using ASTM E447 standard eccentrically-loaded single edge notch tensile (ESE(T)) specimens, are shown in Figure 4.

In this instance, estimated values of ΔK_{th} were given in [85]. These values of ΔK_{th} are reproduced in Table 2. These values of ΔK_{th} can now be used to plot da/dN against $\Delta K/\Delta K_{th}(R)$. The corresponding "normalised plot" is shown in Figure 5, where we also see that when plotted in this fashion the $R = 0.1$ and 0.5 curves again essentially collapse.

These observations, when taken together with Equation (4) and the additional examples given in [81,100] and in and Appendices A and C, support the conclusion reached above that crack growth rate in conventionally manufactured metals would often appear to be primarily controlled by the fatigue threshold.

The observation that for conventionally manufactured metals the R ratio effect on crack growth is, to a first approximation, often reflected in the change of the fatigue threshold ΔK_{th}, is also consistent with the hypothesis first proposed by Hartman and Schijve [66], and also by a number of other subsequent authors [61,67–80], that the crack growth rate (da/dN) should be a function of how much ΔK exceeds its threshold value (ΔK_{th}). This hypothesis, i.e., that the crack growth rate (da/dN) should be a function of how much ΔK exceeds its threshold value, would appear to be supported by the data presented in [4–29,81] for crack

growth in conventionally manufactured, AM and CSAM metals. However, as illustrated in [5–7,11,20], when when using the Hartman-Schijve crack growth equation to model crack growth in AM and CSAM metals it would appear that allowance must also be made for the variability in the fracture toughness that arises due to the manufacturing process used to build the part and the anisotropic nature of AM and CSAM materials.
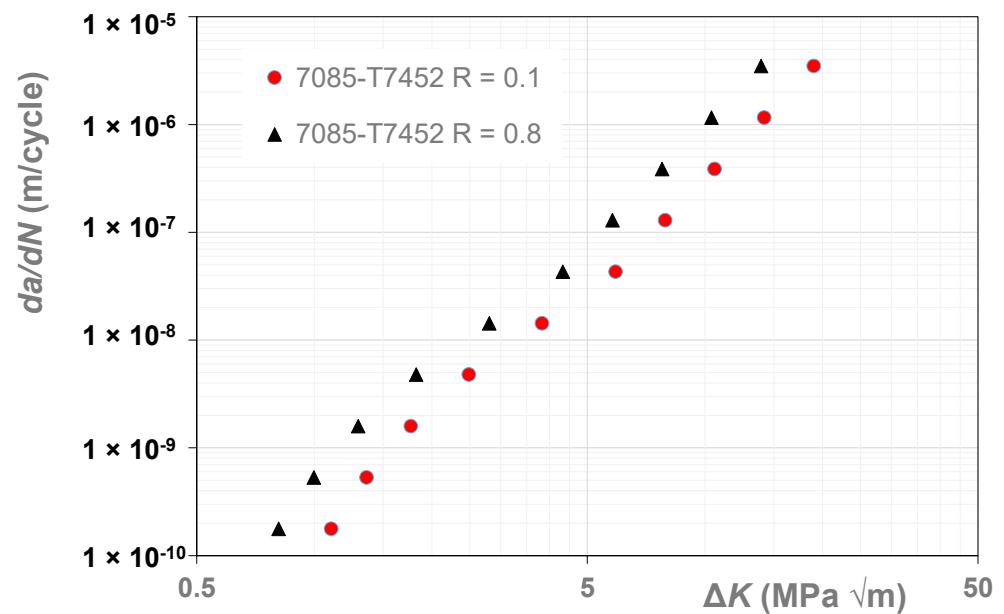

Figure 2. The da/dN versus ΔK curves for the aluminium alloy AA7085-T7452.
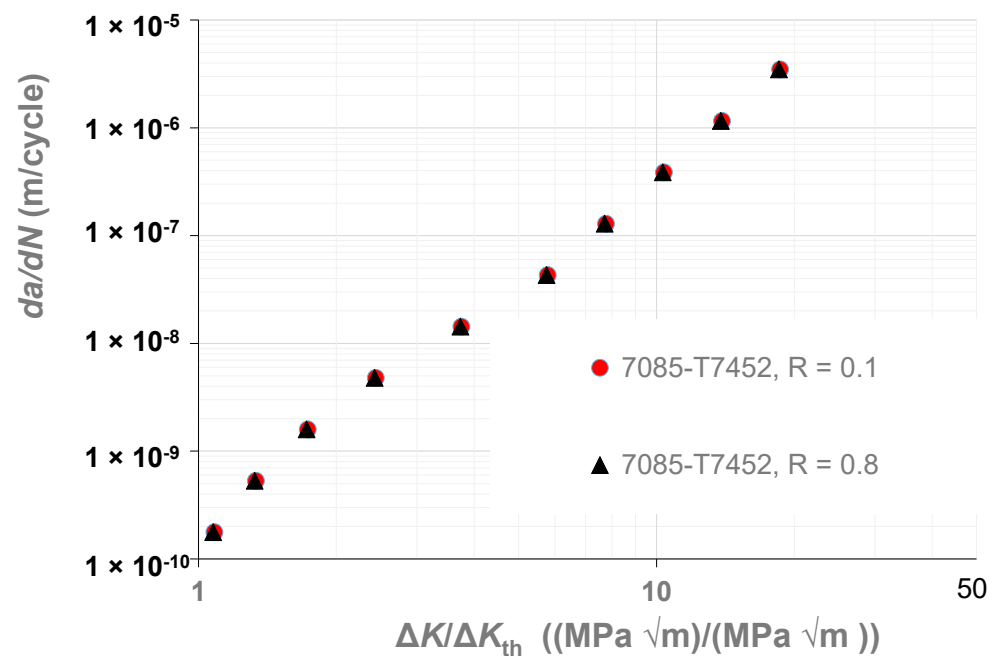

Figure 3. The da/dN versus $\Delta K/\Delta K_{th}$ curves for the aluminium alloy AA7085-T7452.

Table 1. The values of ΔK_{th} used in Figure 3.

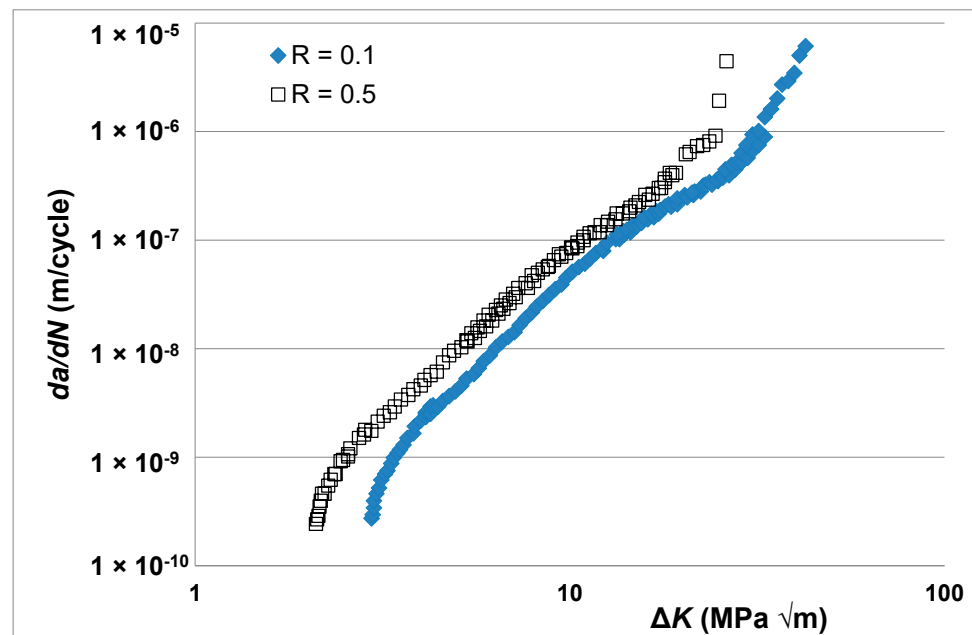| Material and *R* Ratio	ΔK_{th} MPa $\sqrt{m}$
7085-T7452, *R* = 0.1	0.75
7085-T7452, *R* = 0.8	1.02

Figure 4. The *R* = 0.1 and 0.5 *da/dN* versus Δ*K* curves for the titanium alloy Ti-6-2-2-2-2.

Table 2. The values of ΔK_{th} used in Figure 4.

Material and *R* Ratio	ΔK_{th} MPa $\sqrt{m}$
Ti-6-2-2-2-2, *R* = 0.5	2.22
Ti-6-2-2-2-2, *R* = 0.1	3.21

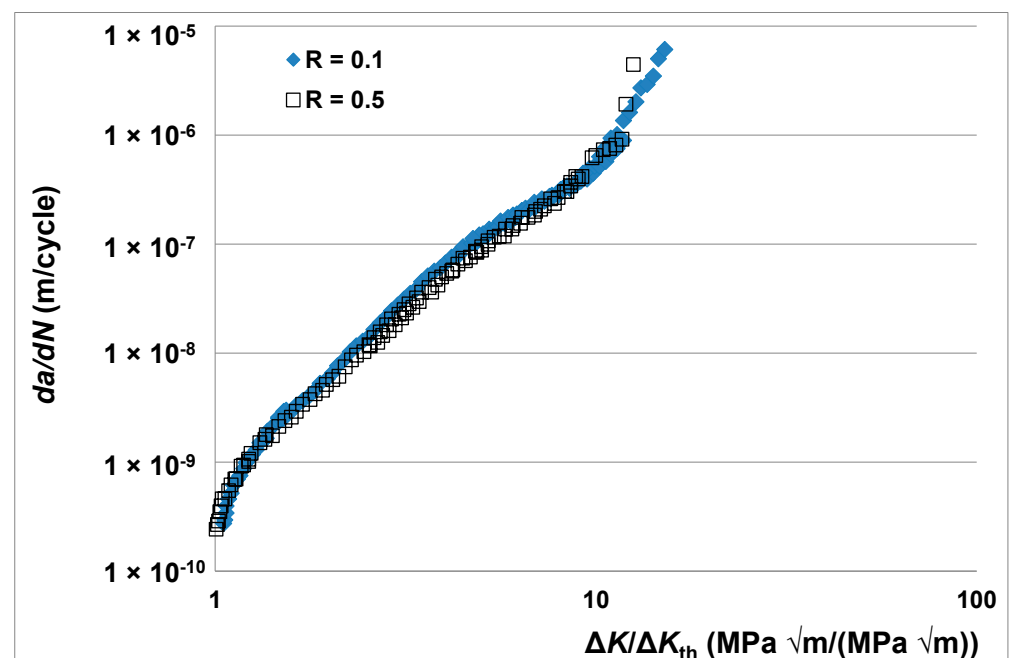**Figure 5.** The *da/dN* versus Δ*K*/ΔK_{th} curves for the titanium alloy Ti-6-2-2-2-2.

4. The Potential to Help Clarify Seemingly Anomalous Behaviour

The paper by Jones et al. [81] also reported that plotting *da/dN* as a function of Δ*K*/ΔK_{th} appeared to have the ability to help understand what, at first glance, appeared to be anomalous *da/dN* versus Δ*K* curves. To further illustrate this let us consider the

da/dN versus K_{max} curves given in [83] for crack growth in underaged (UA) high strength 7049 aluminium alloy tested in air at $R = 0, -1, -2, -3$. These curves, which were obtained using ASTM E647 standard middle tension (MT) specimens,

Here it should be noted that ASTM E647-15el [45] states that for $R \leq 0$ when plotting the da/dN versus ΔK curve the term ΔK can be approximated by K_{max}. As such it is unusual to see that whilst the $R = -1, -2, -3$ curves lie on a single curve the $R = 0$ curve lies on a quite different curve, see Figure 6. However, when these curves are plotted with da/dN expressed as a function of $K_{max}/K_{max,th}$, where $K_{\max,th}$ is the value of K_{max} at a crack growth rate (da/dN) of 10^{-10} m/cycle, then the two different curves collapse onto a single curve, see Figure 7. The values of $K_{\max,th}$ used in Figure 7 are given in Table 3. As such it would appear that, from a mechanics perspective, the reason for the difference shown in Figure 6 is due to the different fatigue threshold that arose when testing at negative R ratio's.
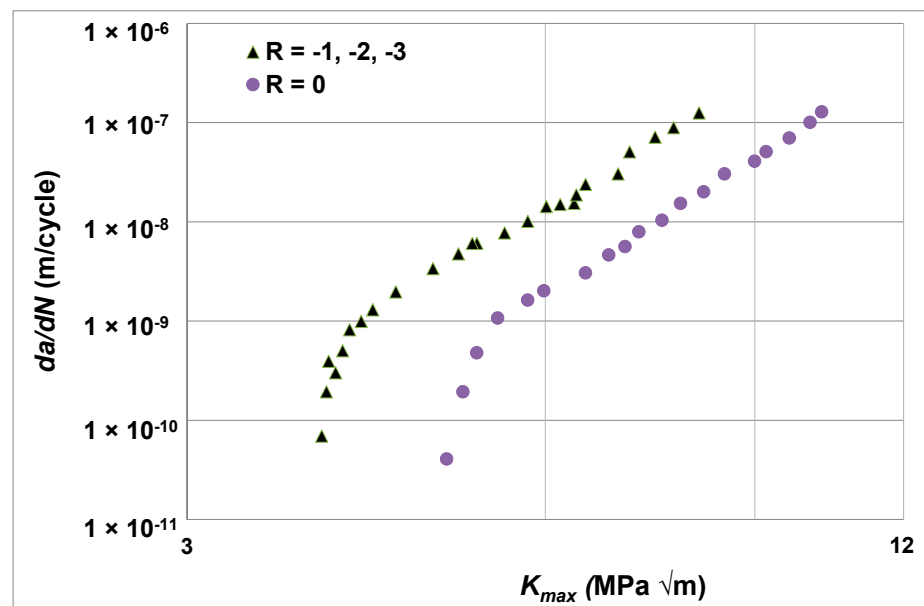

Figure 6. The da/dN versus K_{max} curves for AA7049.
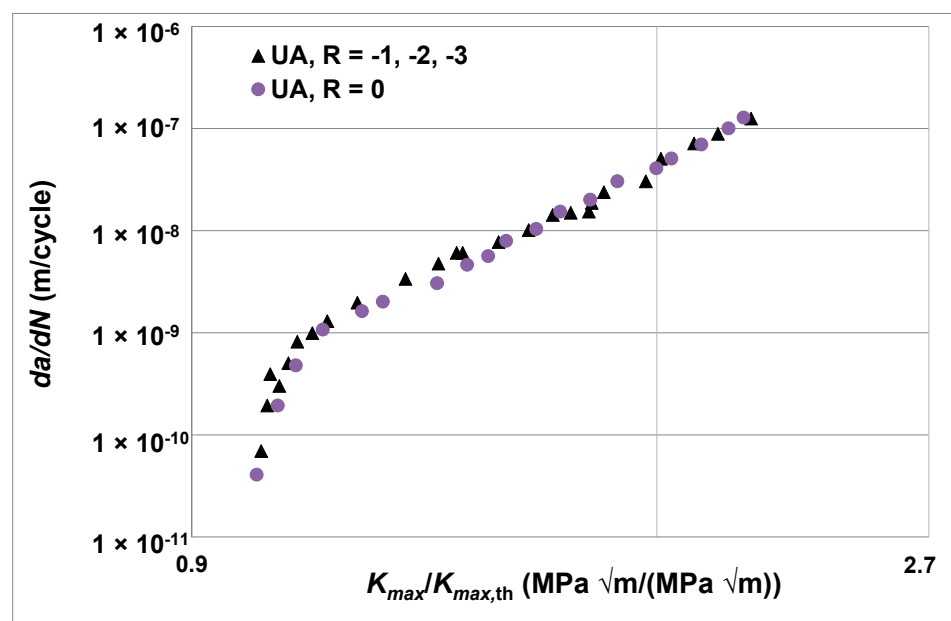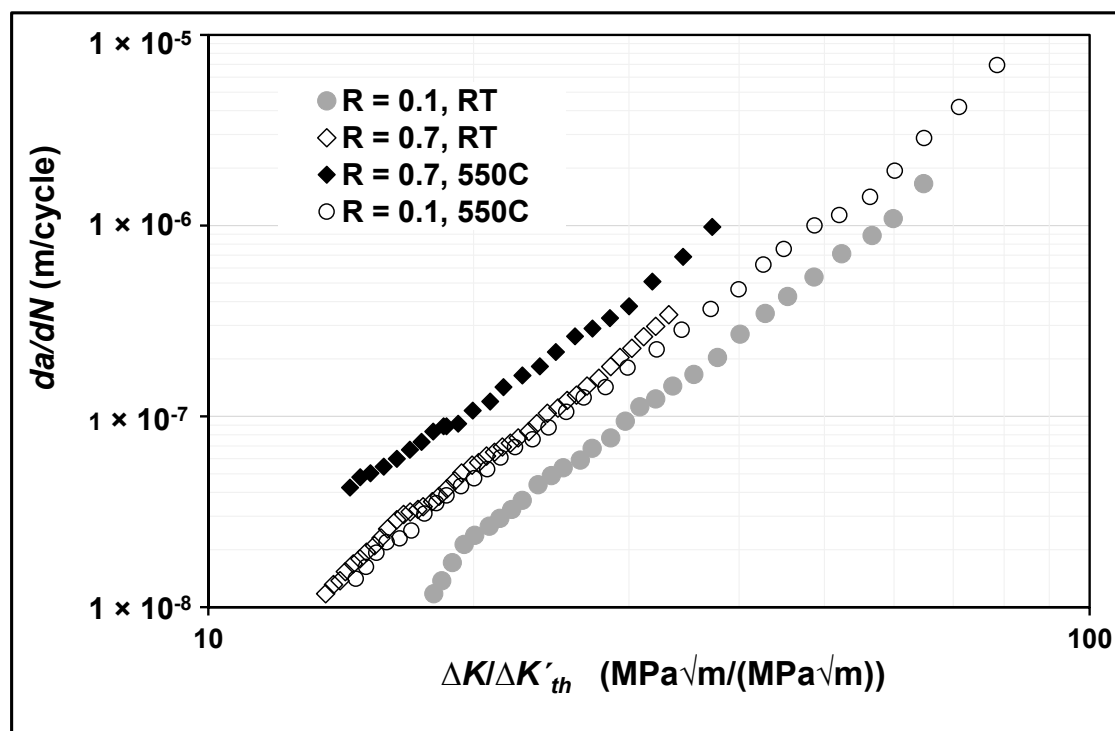

Figure 7. The da/dN versus $K_{max}/K_{\max,th}$ curves for the underaged 7049 tests.

Table 3. The values of $K_{max,th}$ used in Figure 7.

R Ratio	$K_{max,th}$ (MPa $\sqrt{m}$)
R = −1, −2, −3	3.9
R = 0.0	5.0

5. The Potential to Help Clarify Temperature Effects

To continue this study let us next examine the R = 0.1 and 0.7 *da/dN* versus ΔK curves presented in [86] for the growth of cracks in the Ni-based supper alloy GH4169 tested at room temperature (RT) and also at 550 °C. (GH4169 is a Chinese developed superalloy that has similar mechanical properties to Inconel 718 (IN718) [86]). The room temperature and 550 °C R = 0.1 and 0.7 *da/dN* versus ΔK curves are shown in Figure 8. Here we see that the *da/dN* versus ΔK curves are a function of both the test temperature and the R ratio.

Figure 8. The 550°C and RT R = 0.1 and 0.7 *da/dN* versus ΔK curves the super alloy GH4169.

Since Figure 8 does not contain crack growth data beneath a crack growth rate of approximately 10^{-8} m/cycle the various curves were normalised by dividing ΔK by the estimated value of ΔK at a crack growth rate of *da/dN* = 10^{-8} m/cycle, which we will define as $\Delta K'_{th}$. The resultant normalised plots are shown in Figure 9. Interestingly Figure 9 reveals that, when normalised in this fashion, both the R ratio and the temperature dependency effects shown in Figure 8 essentially vanish. In other words, for this material, the temperature and R ratio effects are (to a first approximation) reflected in their effect on a single parameter. Other examples that illustrates how expressing *da/dN* as a function of $\Delta K/\Delta K'_{th}$ can sometimes help when evaluating the effect of temperature on crack growth are given in Appendix C. The values of $\Delta K'_{th}$ used in Figure 9 are given in Table 4.
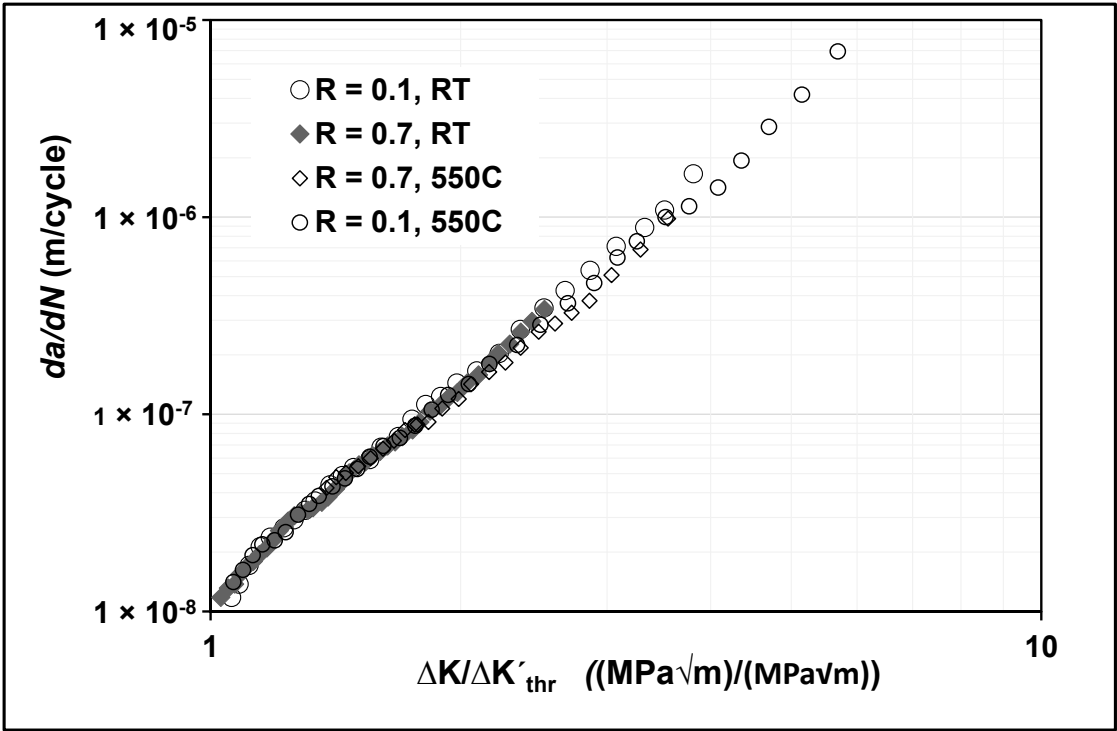
Figure 9. The 550 °C and RT *R* = 0.1 and 0.7 *da/dN* versus ΔK/ΔK′$_{th}$ curves shown in Figures 10 and 11 for the super alloy GH4169.
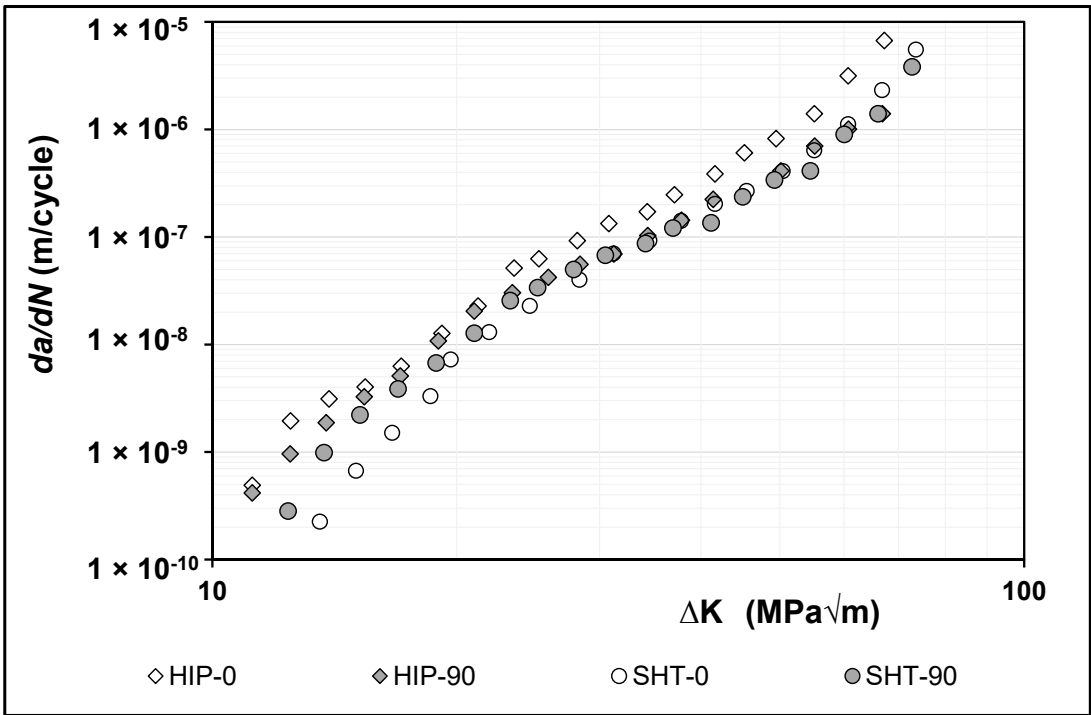

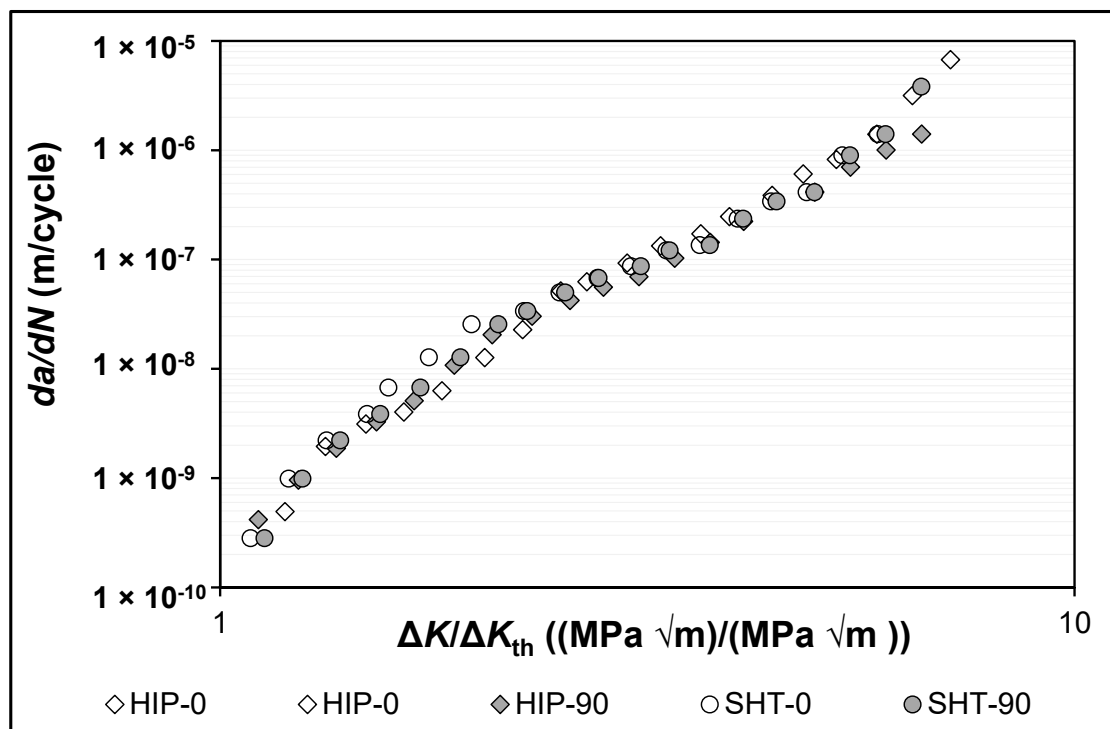**Figure 10.** The *da/dN* versus ΔK curves for LPBF Hastelloy X.

Figure 11. The da/dN versus $\Delta K/\Delta K'_{th}$ curves for LPBF Hastelloy X.

Table 4. The values of $\Delta K'_{th}$ used in Figure 9.

Material, *R* Ratio and Test Temperature	$\Delta K'_{th}$ MPa $\sqrt{m}$
Room temperature tests	
GH4169, *R* = 0.1	17.0
GH4169, *R* = 0.7	13.2
Tests at 550 °C	
GH4169, *R* = 0.1	13.8
GH4169, *R* = 0.7	10.5

6. The Potential to Help Clarify Crack Growth in AM Hastelloy X

We have previously noted that, as previously mentioned, [81] revealed that in the case SLM Inconel 625 plotting da/dN as a function of $\Delta K/\Delta K_{th}$(R) collapses the various *R* ratio dependent da/dN versus ΔK curves onto a single master curve. Consequently. To further investigate the potential for this approach to assit in understanding crack growth in additively manufactured materials we analysed the (room temperature) *R* = 0.1, da/dN versus ΔK curves associated with laser bed powder fusion (LPBF) built ASTM standard CT tests on Hastelloy X where the crack was at either 0° or 90° degrees to the build direction. This paper presented the *R* = 0.1 crack growth curves associated with two different post-build treatments, viz: solution heat treatment (SHT); and hot isostatic pressing (HIP), with the crack at either 0 degress or 90 degress to the build direction.. The resultant the da/dN versus ΔK curves given in [87] are shown in Figure 10.

The corresponding da/dN versus $\Delta K/\Delta K'_{th}$ curves are shown in Figure 11. Figure 11 again appears to suggest that when normalised in this fashion the effect of anisotropy essentially vanishes. The values of $\Delta K'_{th}$ used in Figure 11 are given in Table 5.

Table 5. The values of $\Delta K'_{th}$ used in Figure 11.

Material, Build Direction and *R* Ratio	$\Delta K'_{th}$ MPa $\sqrt{m}$
LPBF Hastelloy X, HIP-0	9.4
LPBF Hastelloy X, HIP-0	10.1
LPBF Hastelloy X, SHT-0	12.5
LPBF Hastelloy X, SHT-90	11.0

7. Brief Summary

Table 6 contains a brief summary of the finding seen in this study. Here we see that in each case expressing da/dN as a function of $\Delta K/\Delta K'_{th}$ appears to have collapsed the various *R* ratio and/or temperature depemdency seen when da/dN vwas expressed as a function of ΔK.

Table 6. Summary Table.

Material, Test Conditions, and Reference	Outcome
7085-T7452 (an aluminum alloy), specimen contained an array of surface notched and was tested at *R* = 0.1 and 0.8, [82].	Expressing da/dN as a function of $\Delta K/\Delta K'_{th}$ essentially collapsed the *R* ratio dependent da/dN versus ΔK curves onto a single curve.
7055 (an aluminium alloy), tested at *R* = 0.75, 0.5, 0.3, and −1, the specimen geometry was not specified, [49.50].	ibid.
2524-T3 (an aluminum alloy), ASTM E647 ESE(T) specimens that were tested at *R* = 0.1, 0.2, 0.3, and 0.5 [83].	ibid.
7049 (aluminium alloy), tested at *R* = 0, −1, −2 and −4, [84].	Expressing da/dN as a function of $\Delta K/\Delta K'_{th}$ essentially removed the anomalous behaviour seen in the *R* ratio dependent da/dN versus K_{max} curves.
The titanium alloy Ti-6-2-2-2-2, an ASTM E647 ESE(T) specimens that were tested at *R* = 0.1 and 0.5, [85].	The *R* ratio depemdency essentially vanished when da/dN was plotted as a function of $\Delta K/\Delta K'_{th}$.
GH4169 (a Chinese super alloy that has mechanical properties similar to Inconel 718), ASTM E647 CT specimens that were tested at *R* = 0.1 and 0.7 at both RT and 550 °C, [86].	Both the *R* ratio and temperature dependent effects essentially vanishwd when da/dN was plotted as a function of $\Delta K/\Delta K'_{th}$.
AM (LPBF) Hastelloy X, an ASTM E647 CT specimens that were either solution heat treated (SHT) or subjected to hot isostatic pressing (HIP) and tested at *R* = 0.1, [87].	The anisotropy seen in the da/dN versus ΔK curves essentially vanished when da/dN was plotted as a function of $\Delta K/\Delta K'_{th}$.
304L stainless steel, ASTM E647 CT specimens tested at cryogenic temperatures and at two different *R* = 0.05 and 0.5 and at RT with *R* = 0.05, [89].	Both the temperature and *R* ratio dependency essentially vanished when da/dN was plotted as a function of $\Delta K/\Delta K'_{th}$.
The medium entropy alloy CrCoNi, an ASTM E647 CT specimens that were tested with *R* = 0.1 and at 77K, 189K and 293K (room temperature), [90].	The effect of the test temperature essentially vanished when da/dN was plotted as a function of $\Delta K/\Delta K'_{th}$.

8. Conclusions

This paper has shown that, whenever Elber's crack closure based approach to modelling crack growth in conventionally manufactured metals is valid, the function $U(R)$ that is used to relate the stress intensity factor ΔK to the effective stress intensity factor ΔK_{eff}, so as to account for plastic wake induced crack closure, would appear to be (to a first approximation) inversely proportional to the fatigue threshold. It thus follows that, in such instances, from a fracture mechanics perspective crack growth in conventionally manufactured metals would often appear to be primarily controlled by the fatigue threshold.

This finding also results in a simple closed-form equation that relates the crack opening stress intensity factor $K_o(R)$, that was originally introduced by Elber, to ΔK, K_{max}, the fatigue thresholds $\Delta K_{th}(R)$ and $\Delta K_{eff,th}$.

At this point it should be restated that this paper does not constitute a proof that *R* ratio effects can always be interpreted as being reflected by its effect on the fatigue threshold. Indeed, there are numerous examples where whilst there are clear *R* ratio effects in the near threshold region this *R* ratio dependency essentially vanishes in the Paris region. Consequently, the discussion presented in this paper is not applicable for such materials. Indeed, the present paper is specifically confined to those materials where Elber's original formulation, by this we mean Equation (2), is a reasonable first approximation. That said, there would appear to be numerous examples where the simplification proposed in this paper would appear to be a reasonable first approximation.

It is also shown that plotting da/dN as function of against $\Delta K/\Delta K_{th}(R)$ would appear to have the potential to help identify the key fracture mechanics parameters that characterise the effect of the test temperature on crack growth. However, it should be stressed that this may not always be the case. Nevertheless, replotting the da/dN versus $\Delta K(R)$ curve with da/dN plotted as function of against $\Delta K/\Delta K_{th}(R)$ would appear to be a useful additional approach to help to identify the (fracture mechanics based) parameters affecting crack growth.

In the case of the annealed SLM Inconel 625 tests and the various $R = 0.1$ tests on LPBF Hastelloy X specimens that are examined in this study it would appear that plotting da/dN versus $\Delta K/\Delta K_{th}$ may also help to identify the fracture mechanics parameters that characterise the effect of the build direction on crack growth in AM materials. However, it should be stressed that further work is needed to investigate if this hypothesis holds for other AM materials.

Data Availability Statement: The data presented in this study are available on request from the corresponding author. The data are not publicly available due to the ongoing nature of the study.

Conflicts of Interest: The authors declare no conflict of interest.

Nomenclature

Material and *R* ratio	ΔK_{th} MPa $\sqrt{m}$
a	crack length
AM	additive manufacturing
ASTM	American Society for Testing and Materials (ASTM)
da/dN	the increment in the crack length per cycle
DADT	durability and damage tolerance
G	the energy release rate
G_{max}	the maximun value of *G* in a load cycle
G_{min}	the minimun value of *G* in a load cycle
$\Delta \sqrt{G}$	range of $\sqrt{G}$ in a fatigue cycle, as defined below$\Delta \sqrt{G} = \sqrt{G_{max}} - K\sqrt{G_{min}}$
$\Delta \sqrt{G_{th}}$	the value of $\Delta \sqrt{G}$ at a crack growth rate (da/dN) of 10^{-10} m/cycle
$\Delta \sqrt{G_{eff}}$	the crack closure corrected value of $\Delta \sqrt{G}$
$\Delta \sqrt{G_{eff,th}}$	the value of $\Delta \sqrt{G_{eff}}$ at a crack growth rate (da/dN) of 10^{-10} m/cycle
$G_o(R)$	the value of *G* at which the crack first opens
K	stress-intensity factor
K_{max}	the maximun value of *K* in a load cycle

K_{min}	the minimun value of K in a load cycle
ΔK	range of the applied stress-intensity factor in the fatigue cycle, as defined below $\Delta K = K_{max} - K_{min}$
ΔK_{th}	the value of ΔK at a crack growth rate (da/dN) of 10^{-10} m/cycle
$\Delta K'_{th}$	the value of ΔK at a low crack growth rate, typically $da/dN = 10^{-8}$ m/cycle
ΔK_{eff}	The crack closure corrected value of ΔK that is defined as $\Delta K_{eff} = U(R)\,\Delta K$
$\Delta K_{eff,th}$	the value of ΔK_{eff} at a crack growth rate (da/dN) of 10^{-10} m/cycle
$K_o(R)$	the value of K at which the crack first opens
$\Delta K_{2/\pi 0}$,	an alternative formulation for the crack closure corrected value of ΔK, namely $\Delta K_{2/\pi 0} = (K_{max} - 2K_o(R)/\pi)$
$\Delta \kappa$	the Schwalbe crack driving force
LBPF	laser bed powder fusion, an additive manufacturing process
LEFM	linear-elastic fracture-mechanics
R	the R ratio, defined as $R = K_{min}/K_{max}$
SLM	Selective laser melting, an additive manuring process
$U(R)$	Elber's crack closue function that relates ΔK to ΔK_{eff}, viz: $U(R) = (K_{max} - K_o(R))/(K_{max} - K_{min})$
USA	United States of America
USAF	United States Air Force

Appendix A

Whilst, as shown in [52,53,55], Elber's [47] statement that for plasticity induced crack closure the function U is essentially only a function of *R* is supported by numerous studies there are also studies that suggest otherwise, see [48–52]. Unfortunately, as illustrated in [91.95] and in Appendix B, the load reducing test protocol described in the ASTM Fatigue Test Standard ASTM E647-15el [45] can sometimes lead to erroneous *da/dN* versus ΔK curves. The problem of assessing Elber's the validity of original hypothesis is further complicated by:

(i) The variability in the measured *da/dN* versus ΔK curves that is known to be associated with repeat tests [22,101];

(ii) The level of experimental error that is often associated with the crack growth rates, particularly at low crack growth rates. The experimental data presented in [52] is a good example of the latter;

(iii) The need, as delineated by Paris et al. [50], for precise computer controlled load-displacement data.

Consequently, it is sometimes difficult to make a statement with respect to the voracity or otherwise of Elber's hypothesis that U is essentially only a function of the *R* ratio. However, in light of the data given in [52,53,55], which suggest that to a first approximation U is often essentially only a function of *R*, and given that [81,84] have shown that there are a number of examples where the experimental data reveals that U can often be reasonably well approximated as being inversely proportional to ΔK_{th}, the present paper suggests that Elber's statement may often represent a reasonable first approximation.

Nevertheless, it also should be emphasised that the findings outlined in the present paper, that expressing *da/dN* as function of $\Delta K/\Delta K_{th}(R)$ would appear to have the potential to help identify the fracture mechanics based parameters that characterise crack growth, are (in theory) specifically confined to those materials where Elber's original formulation, i.e., Equation (2), is a reasonable first approximation.

Let us now return to the question of crack closure and the *R* ratio dependency of the *da/dN* versus ΔK curves. References [49,50] gave a number of examples where whilst expressing *da/dN* as a function of $(K_{max} - K_o(R))$ helped collapse the various curves in region where *da/dN* was greater than approximately 10^{-8} m/cycle this was not the case for the region where *da/dN* was less than approximately 10^{-8} m/cycle. Whilst [49,50] revealed an improvement could be achieved by representing *da/dN* as a function of both K_{max} and $(K_{max} - K_o(R))$ they reported that the best result was achieved by plotting *da/dN* as a function of $\Delta K_{2/\pi 0}$.

In this context, it should be noted that reference [81] illustrated that the various *R* ratio dependent crack growth curves given in [49,50] for the aluminium alloys 6013-T651 and 2324-T39 collapsed if *da/dN* was plotted as a function of $\Delta K / \Delta K_{th}$. However, [49,50] also presented data for the aluminium alloy 7055. Neither the heat treatment or the nature of the specimen geometry was given in [49,50]. The *R* = 0.75, 0.5, 0.3, and −1 *da/dN* versus ΔK curves given in [49,50] for this alloy are shown in Figure A1. Since not all curves have crack growth data at 10^{-10} m/cycle the various curves were normalised by dividing ΔK by its estimated value at a crack growth rate of *da/dN* = 10^{-8} m/cycle, which we will define as $\Delta K'_{th}$. The resultant normalised plots are shown in Figure A2 where we see that, to a first approximation, the various (normalised) *R* ratio dependent curves also collapse. Consequently, for this material, the *R* ratio effects shown in Figure A1 would appear to be (to a first approximation) reflected by their effect on the fatigue threshold.

Table A1. The values of $\Delta K'_{th}$ used in Figure A1.

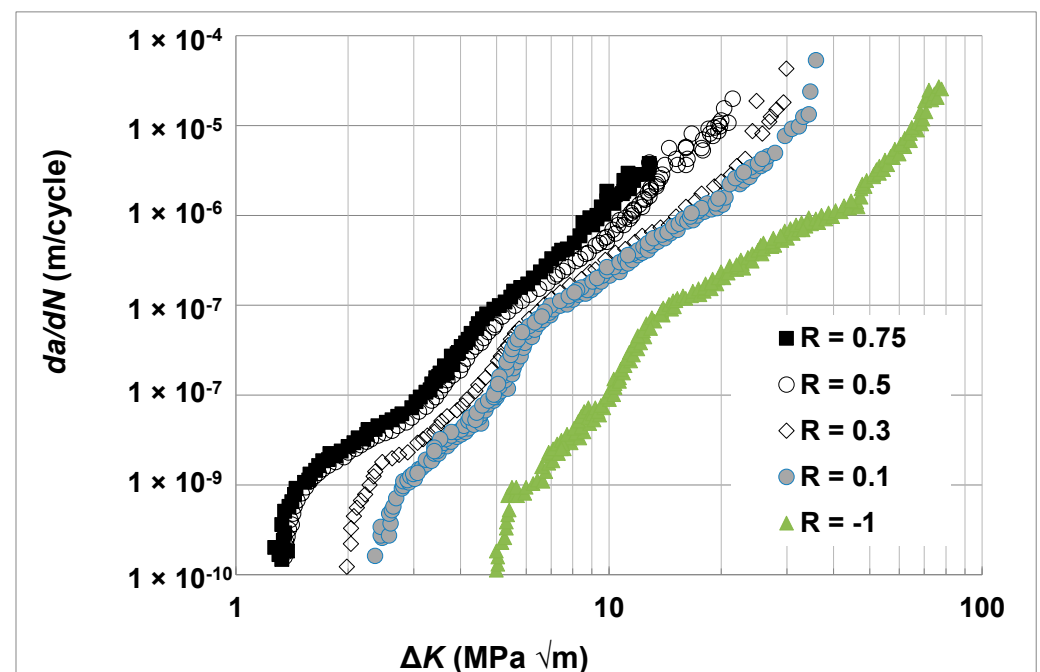| *R* Ratio	$\Delta K'_{th}$ MPa $\sqrt{m}$
R = 0.75	3.0
R = 0.5	3.5
R = 0.3	4.3
R = 0.1	5.0
R = −1	10.2

Figure A1. The *R* = 0.75, 0.5, 0.3, and −1 *da/dN* versus ΔK curves for the aluminium alloy 7055.
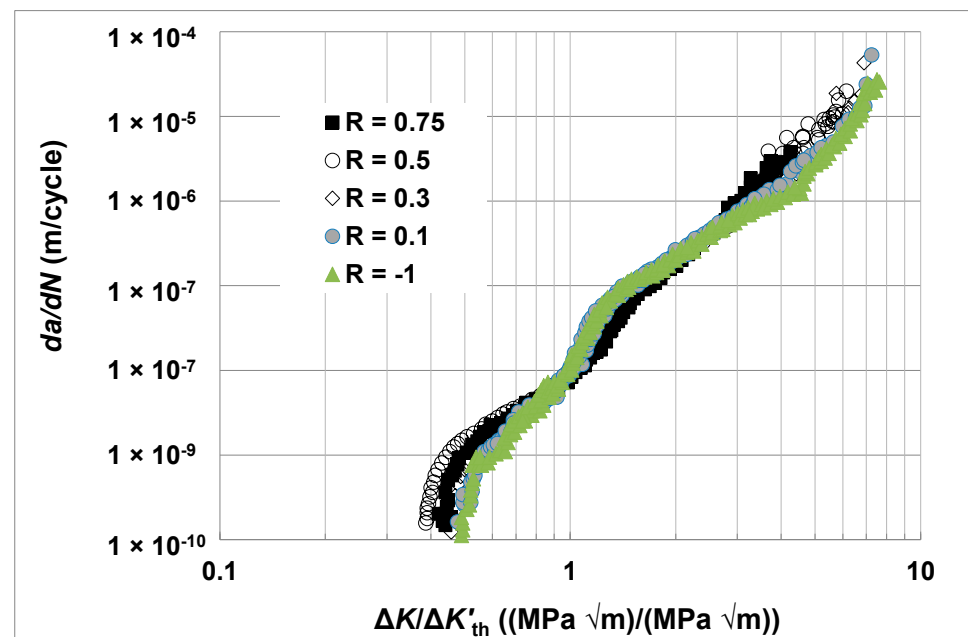
Figure A2. The R = 0.75, 0.5, 0.3, 0.1 and -15 da/dN versus $\Delta K/\Delta K'_{th}$ curves for the aluminium alloy 7055.

That the purpose of this particular example is not to suggest that whenever the function U would appear to be a function of both K_{max} and R the curves will nevertheless collapse if da/dN was plotted as a function of $\Delta K/\Delta K_{th}$. However, as illustrated above, there are cases when it will. As such, evaluationg if this concept holds would appear to be a useful addition to the tools available to assess the fracture mechanics parameters affecting crack growth.

Appendix B

It is now known [61,91–94] that the ASTM load reducing test protocol can results in da/dN versus ΔK curves that are dependent on the specimen test geometry. Furthermore, it is also known [101] that, for a given specimen geometry, even if both the loads and the starting crack size are tightly controlled the da/dN versus ΔK curve is not necessarily unique. (This observation is supported by the test data discussed in [22,102]). As a result of these and related observations, the NASA Fracture Control Handbook NASA-HDBK-5010 [103] mandates the use of the worst case da/dN versus ΔK curve.

These observations complicate our assessment of the suggestion that, to the best of the author's knowledge was first delineated in [84], that for long cracks the function $U(R)$ could be a function of both R and K_{max}. Consequently, the present paper is focused on those data sets that would appear to conform to Equation (2).

At this point, it should also be noted that the present paper does not propose to advocate either for or against the use of crack closure based crack growth equations. It's purpose is to:

(i)   Examine the relationship between Elber's original equation, i.e., Equation (2), and those equations that are based on the assumption that crack growth is a function of how much ΔK exceeds the fatigue crack growth threshold;

(ii) Present a new tool to help assess the fracture mechanics parameters affecting crack growth.

Appendix C. Additional Examples

To further illustrate this phenomenon let us consider the R = 0. 1, 0.2, 0.3, and 0.5 da/dN versus ΔK curves presented in [83] for the aluminium alloy 2524-T3. These curves, which were obtained using ASTM E647-15el standard compact tension (CT) specimens, are shown

in Figure A3. Since Figure A3 does not contain crack growth data beneath 10^{-8} m/cycle the various curves were normalised by dividing ΔK by the estimated value of at a crack growth rate of $da/dN = 10^{-8}$ m/cycle, which we will define as $\Delta K'_{th}$. The resultant normalised plots are shown in Figure A4 where we see that, to a first approximation, the various (normalised) R ratio curves also collapse. The values of $\Delta K'_{th}(R)$ used in Figure A4 are listed in Table A2. Consequently, it would appear that, to a first approximation, the R ratio effects shown in Figure A3 are reflected by their effect on the fatigue threshold.
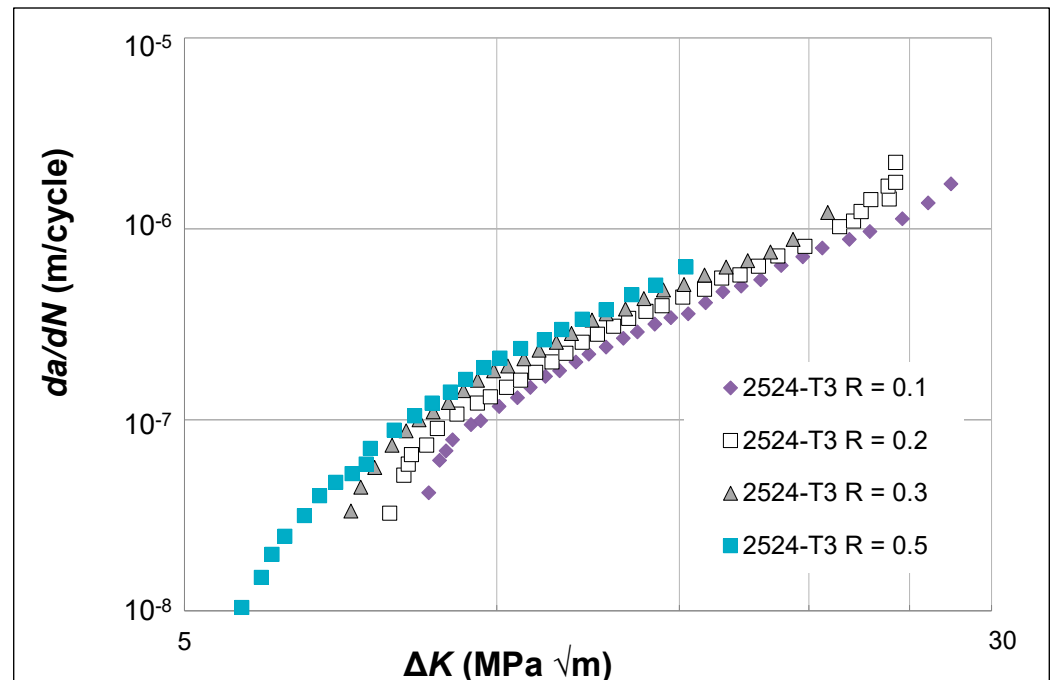

Figure A3. The R =0.1, 0.2, 0.3 and 0.5 da/dN versus ΔK curves for the aluminium alloy AA2524-T3.
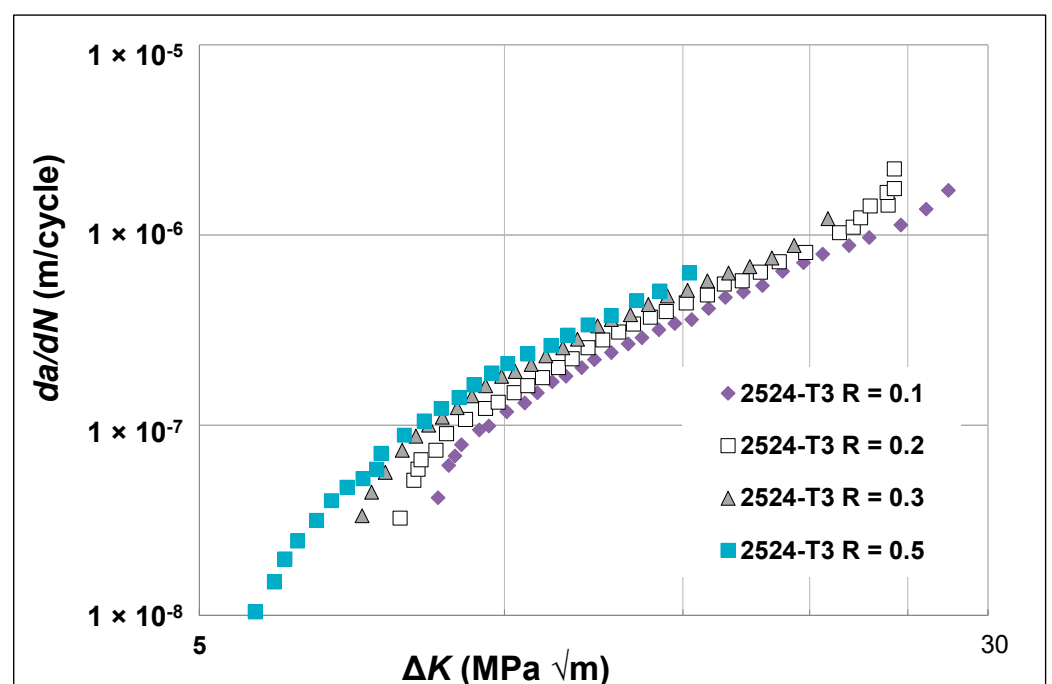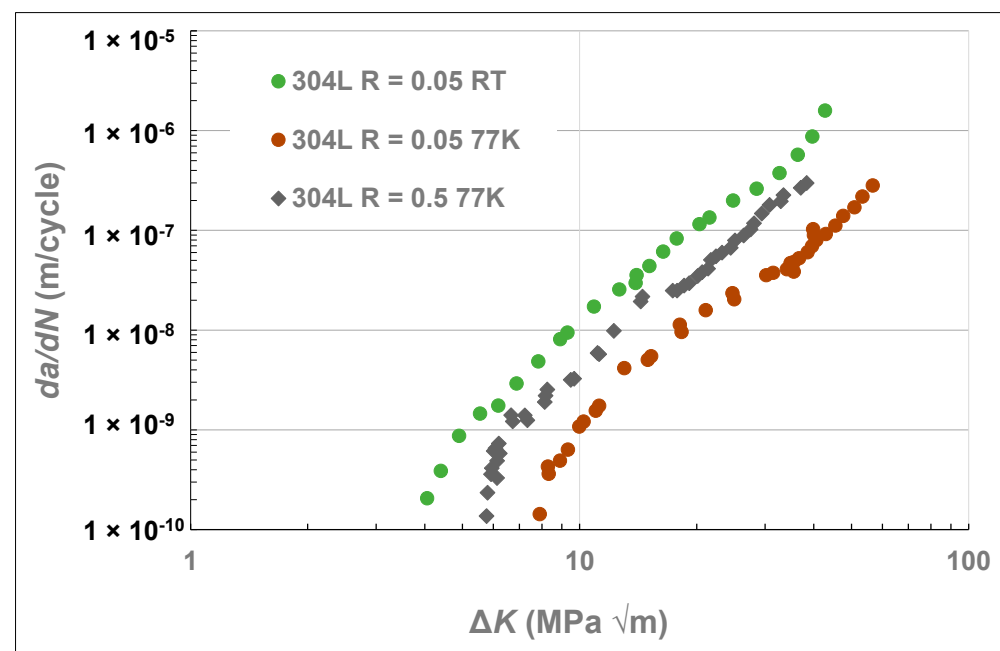

Figure A4. The R = 0.1, 0.2, 0.3 and 0.5 da/dN versus $\Delta K/\Delta K'_{th}$ curves for the aluminium alloy AA2524-T3.

Table A2. The values of $\Delta K'_{th}$ used in Figure A4.

R Ratio	$\Delta K'_{th}$ MPa $\sqrt{m}$
R = 0.1	6.6
R = 0.2	6.3
R = 0.3	5.9
R = 0.5	5.6

To continue this study let us next consider the *R* = 0.05 and 0.5 *da/dN* versus ΔK curves presented in [89] for crack growth in 304L stainless steel tested at cryogenic temperatures (77K) and the *R* = 0.05 *da/dN* versus ΔK curve presented in [89] for crack growth in 304L stainless steel at room temperature (RT). These curves, which were obtained using ASTM E647 standard compact tension (CT) specimens, are reproduced in Figure A5.

Figure A5 reveals that the *da/dN* versus ΔK curves are functions of both the test temperature and the *R* ratio. Figure A6 reveals that when *da/dN* is plotted as function of $\Delta K/\Delta K_{th}(R)$ then, to a first approximation, these curves also essentially collapse onto a single curve. In other words, for this material, the *R* ratio and temperature dependencies seen in Figure A5 are (to a first approximation) reflected by their effect on a single parameter. The values of $\Delta K_{th}(R)$ used in Figure A6 are listed in Table A3.

Figure A5. The *da/dN* versus ΔK curves for 304L stainless steel tested at room temperature and 77 K.

To further illustrate the potential advantages of plotting *da/dN* as function of $\Delta K/\Delta K_{th}(R)$ let us examine the *R* = 0.1 *da/dN* versus ΔK curves presented in [90]. for the 7 μm (fine grained) medium entropy alloy (MEA) CrCoNi tested at 77 K, 189 K and 293 K (room temperature), see Figure A7. These curves were obtained using disk-shaped compact-tension DC(T) specimens. The *da/dN* versus $\Delta K/\Delta K_{th}(R)$ curves associated with these test temperatures are shown in Figure A8. Here we again see that, to a first approximation, when plotted in this fashion the effect of the test temperature essentially vanishes. In other words, for this *R* ratio, the temperature dependencies seen in Figure A5 are (to a first approximation) reflected by their effect on a single parameter. The values of $\Delta K_{th}(R)$ used in Figure A8 are given in Table A4.
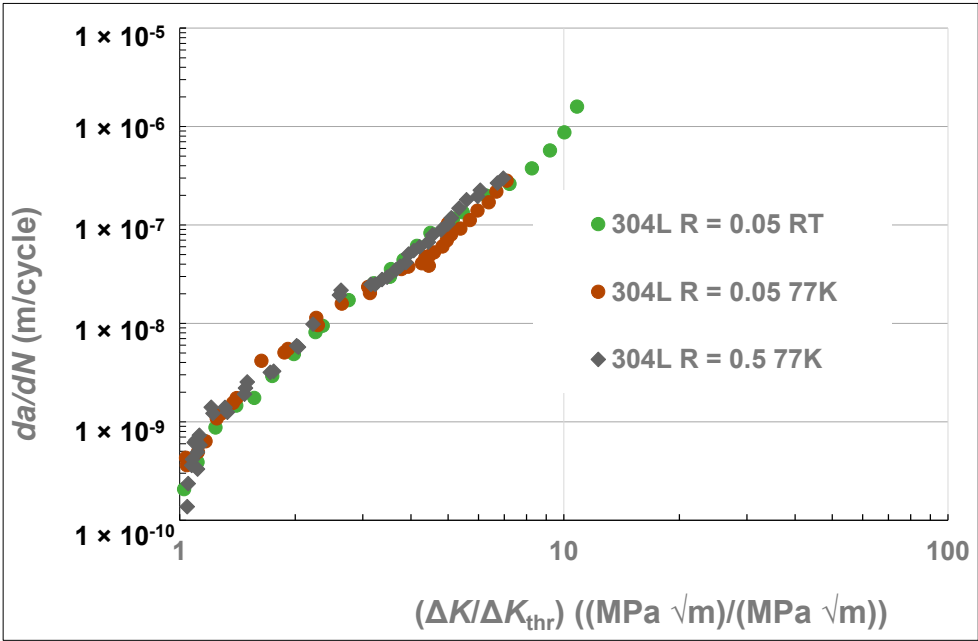
Figure A6. The *da/dN* versus $\Delta K/\Delta K'_{th}$ curves for 304L stainless steel tested at room temperature and 77K.

Table A3. The values of ΔK_{th} used in Figure A6.

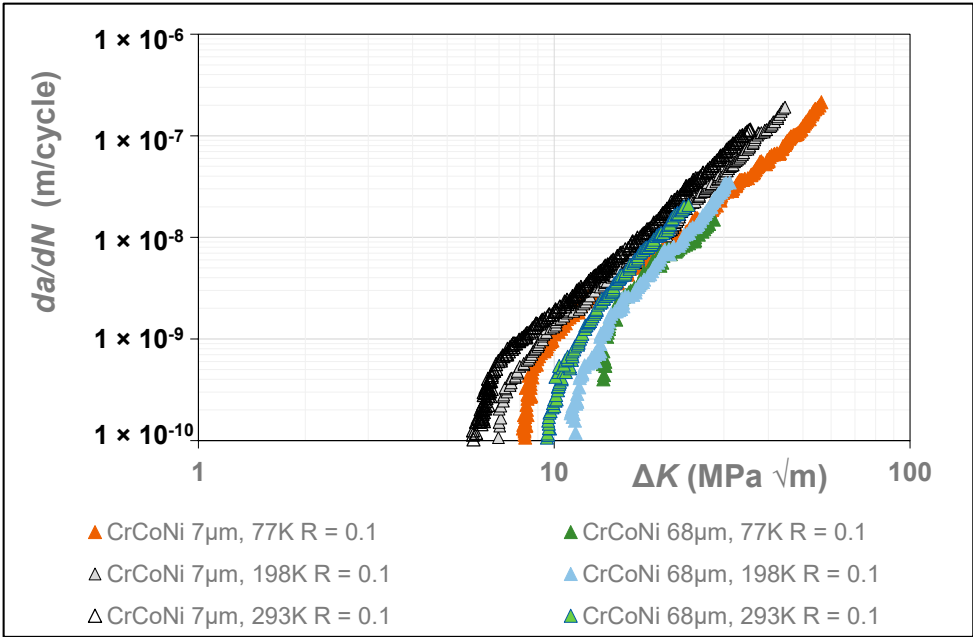| Material, *R* Ratio and Test Temperature	ΔK_{th} MPa $\sqrt{m}$
304L, *R* = 0.5, 77 K	5.5
304L, *R* = 0.05, 77 K	8.0
304L, *R* = 0.05, RT	4.0

Figure A7. The *R* = 0.1 *da/dN* versus ΔK curves for 7 μm (fine grained) medium entropy alloy (MEA) CrCoNi tested at 77 K, 189 K and 293 K (room temperature).
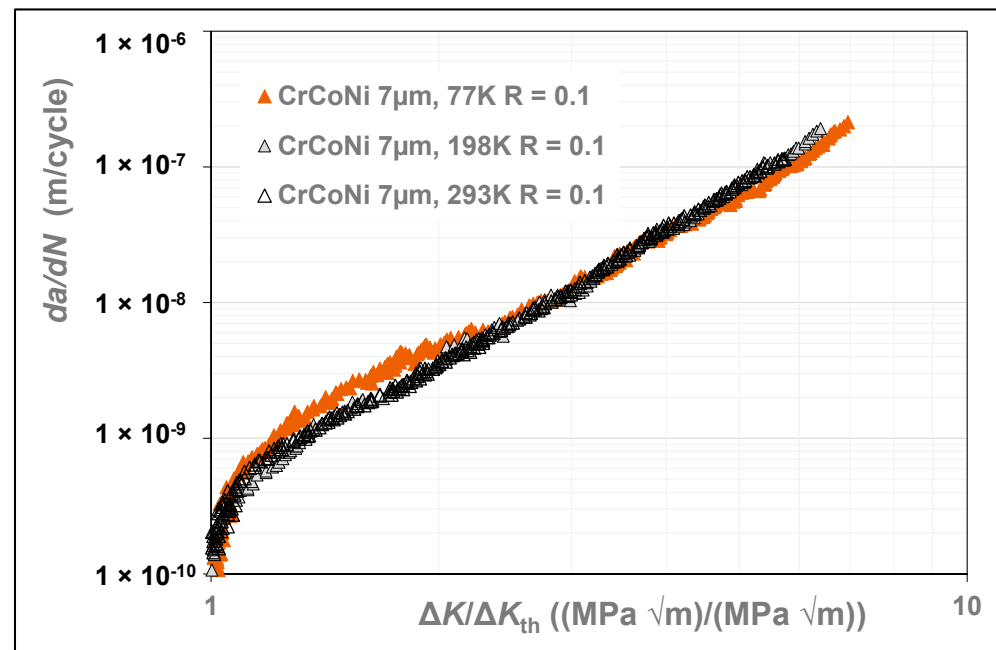
Figure A8. The $R = 0.1$ *da/dN* versus $\Delta K/\Delta K_{th}$ curves for the MEA CrCoNi tested at 77 K, 189 K and 293 K.

Table A4. The values of ΔK_{th} used in Figure A8.

Test Temperature	ΔK_{th} MPa $\sqrt{m}$
77 K	8.1
189 K	7.0
293 K (RT)	6.2

References

1. Davis, S.L.; DeGood, K.; Donohue, N.; Goldberg, D. The Fix We're In For: The State of Our Nation's Busiest Bridges, Transportation for America. 2013. Available online: http://t4america.org/docs/bridgereport2013/2013BridgeReport.pdf (accessed on 20 April 2024).
2. MIL-STD-1530D, Department of Defense Standard Practice Aircraft Structural Integrity Program (ASIP), 13 October 2016. Available online: http://everyspec.com/MIL-STD/MIL-STD-1500-1599/MIL-STD-1530D_55392/ (accessed on 12 April 2024).
3. Structures Bulletin EZ-SB-19-01, Durability and Damage Tolerance Certification for Additive Manufacturing of Aircraft Structural Metallic Parts, Wright Patterson Air Force Base, OH, USA, 10 June 2019. Available online: https://daytonaero.com/usaf-structures-bulletins-library/ (accessed on 12 April 2024).
4. Ye, J.; Syed, A.K.; Zhang, X.; Eimer, E.; Williams, S. Fatigue crack growth behaviour in an aluminium alloy Al-Mg-0.3Sc produced by wire based directed energy deposition process. *Fatigue Fract. Eng. Mater. Struct.* **2023**, *46*, 3927–3938. Available online: https://onlinelibrary.wiley.com/doi/epdf/10.1111/ffe.14113 (accessed on 20 April 2024). [CrossRef]
5. Jones, R.; Ang, A.; Peng, D.; Champagne, V.K.; Michelson, A.; Birt, A. Modelling Crack Growth in Additively Manufactured Inconel 718 and Inconel 625. *Metals* **2023**, *13*, 1300. [CrossRef]
6. Iliopoulos, A.P.; Jones, R.; Michopoulos, J.G.; Phan, N.; Singh Raman, R.K. Crack growth in a range of additively manufactured aerospace structural materials, Special Issue, Civil and Military Airworthiness: Recent Developments and Challenges. *Aerospace* **2019**, *4*, 118. [CrossRef]
7. Jones, R.; Rans, C.; Iliopoulos, A.P.; Michopoulos, J.G.; Phan, N.; Peng, D. Modelling the variability and the anisotropic behaviour of crack growth in SLM Ti6Al4V. *Materials* **2021**, *14*, 1400. [CrossRef] [PubMed]
8. Peng, D.; Jones, R.; Ang, A.S.M.; Michelson, A.; Champagne, V.; Birt, A.; Pinches, S.; Kundu, S.; Alankar, A.; Singh Raman, R.K. Computing the durability of WAAM 18Ni 250 Maraging steel specimens. *Fatigue Fract. Eng. Mater. Struct.* **2022**, *45*, 3535–3545. [CrossRef]
9. Han, S.; Dung Dinh, T.; De Baere, I.; Boone, M.; Josipovic, I.; Van Paepegem, W. Study of the effect of defects on fatigue life prediction of additive manufactured Ti-6Al-4V by combined use of micro-computed tomography and fracture-mechanics-based simulation. *Int. J. Fatigue* **2023**, *180*, 108110. [CrossRef]

10. Shamir, M.; Zhang, X.; Syed, A.K. Characterising and representing small crack growth in an additive manufactured titanium alloy. *Eng. Fract. Mech.* **2021**, *253*, 107876. [CrossRef]
11. Jones, R.; Michopoulos, J.G.; Iliopoulos, A.P.; Singh Raman, R.K.; Phan, N.; Nguyen, T. Representing Crack Growth In Additively Manufactured TI-6AL-4V. *Int. J. Fatigue* **2018**, *111*, 610–622. [CrossRef]
12. Jones, R.; Cizek, J.; Kovarik, O.; Ang, A.; Champagne, V. Observations on comparable aluminium alloy crack growth curves: Additively manufactured Scalmalloy®as an alternative to AA5754 and AA6061-T6 alloys? *Addit. Manuf. Lett.* **2022**, *2*, 100026. [CrossRef]
13. Sanaei, N.; Fatemi, A. Defect-based multiaxial fatigue life prediction of L-PBF additive manufactured metals. *Fatigue Fract. Eng. Mater. Struct.* **2021**, *44*, 1897. [CrossRef]
14. Sanaei, N.; Fatemi, A. Defect-based fatigue life prediction of L-PBF additive manufactured metals. *Eng. Fract. Mech.* **2021**, *244*, 107541. [CrossRef]
15. Markham, M.J.; Fatemi, A.; Phan, N. Mixed-Mode Small Fatigue Crack Growth Rates and Modeling in Additively Manufactured Metals. *Int. J. Fatigue* **2024**, *183*, 108258. [CrossRef]
16. Sanaei, N.; Fatemi, A. Defects in additive manufactured metals and their effect on fatigue performance: A state-of-the-art review. *Prog. Mater. Sci.* **2021**, *117*, 100724. [CrossRef]
17. Dastgerdi, J.N.; Jaberi, O.; Remes, H.; Lehto, P.; Toudeshky, H.H.; Kuva, J. Fatigue damage process of additively manufactured 316L steel using X-ray computed tomography imaging. *Addit. Manuf.* **2023**, *70*, 103559. [CrossRef]
18. Markham, M.J.; Fatemi, A. Multiaxial Fatigue Life Predictions of Additively Manufactured Metals using a Hybrid of Linear Elastic Fracture Mechanics and a Critical Plane Approach. *Int. J. Fatigue* **2024**, *178*, 107979. [CrossRef]
19. Peng, D.; Champagne, V.K.; Ang, A.S.M.; Birt, A.; Michelson, A.; Pinches, S.; Jones, R. Computing the Durability of WAAM 18Ni-250 Maraging Steel Specimens with Surface Breaking Porosity. *Crystals* **2023**, *13*, 443. [CrossRef]
20. Jones, R.; Kovarik, O.; Bagherifard, S.; Cizek, J.; Lang, J. Damage tolerance assessment of AM 304L and cold spray fabricated 316L steels and its implications for attritable aircraft. *Eng. Fract. Mech. Eng. Fract. Mech.* **2021**, *254*, 107916. [CrossRef]
21. Schwalbe, K.H. On the Beauty of Analytical Models for Fatigue Crack Propagation and Fracture-A Personal Historical Review. *J. ASTM Intl.* **2010**, *7*, 3–73. [CrossRef]
22. Molent, L.; Jones, R. The influence of cyclic stress intensity threshold on fatigue life scatter. *Int. J. Fatigue* **2016**, *82*, 748–756. [CrossRef]
23. Molent, L. *Aircraft Fatigue Management*; Springer Briefs in Applied Sciences and Technology; Springer Nature Singapore Pty Ltd.: Berlin/Heidelberg, Germany, 2023; ISBN 978-981-99-7467-2, ISBN 978-981-99-7468-9 (eBook). [CrossRef]
24. Zhang, Y.; Zheng, K.; Heng, J.; Zhu, J. Corrosion-Fatigue Evaluation of Uncoated Weathering Steel Bridges. *Appl. Sci.* **2019**, *9*, 3461. [CrossRef]
25. Wanhill, R.J.H.; Stanzl-Tschegg, S.E. Short/small fatigue crack growth, thresholds and environmental effects: A tale of two engineering paradigms. *Corros. Rev.* **2021**, *39*, 165–175. [CrossRef]
26. Main, B.; Evans, R.; Walker, K.; Yu, X.; Molent, L. Lessons from a fatigue prediction challenge for an aircraft wing shear tie post. *Int. J. Fatigue* **2019**, *123*, 53. [CrossRef]
27. Tan, J.L.; Chen, B.K. Prediction of fatigue life in aluminum alloy (AA7050-T7451) structures in the presence of multiple artificial short cracks. *Theor. Appl. Fract. Mech.* **2015**, *78*, 1–7. [CrossRef]
28. Godefroid, L.B.; Moreira, L.P.; Vilela, T.C.G.; Faria, G.L.; Candido, L.C.; Pinto, E.S. Effect of chemical composition and microstructure on the fatigue crack growth resistance of pearlitic steels for railroad application. *Int. J. Fatigue* **2019**, *120*, 241. [CrossRef]
29. Tan, J.L.; Chen, B.K. A new fracture area method for predicting the growth of a newly coalesced crack in AA7050-T7451 aluminium alloy. *Theor. Appl. Fract. Mech.* **2015**, *75*, 146–150. [CrossRef]
30. Kovarik, O.; Cizek, J.; Klecka, J. Fatigue Crack Growth Rate Description of RF-Plasma-Sprayed Refractory Metals and Alloys. *Materials* **2023**, *16*, 1713. [CrossRef]
31. Khudiakova, A.; Brunner, A.J.; Wolfahrt, M.; Pinter, G. Quantification Approaches for Fatigue Crack Resistance of Thermoplastic Tape Layered Composites with Multiple Delaminations. *Materials* **2021**, *14*, 1476. [CrossRef]
32. Riedl, G.; Pugstaller, R.; Wallner, G.M. Development and implementation of a simultaneous fatigue crack growth test setup for polymeric hybrid laminates. *Eng. Fract. Mech.* **2002**, *267*, 108468. [CrossRef]
33. Simon, I.; Banks-Sills, L.; Fourman, V. Mode I delamination propagation and R-ratio effects in woven DCB specimens for a multi-directional layup. *Int. J. Fatigue* **2017**, *96*, 237–251. [CrossRef]
34. Arhant, M.; Lolive, E.; Bonnemains, T.; Davies, P. Effect of aging on the fatigue crack growth properties of carbon-polyamide 6 thermoplastic composites using the multi ΔG-control method. *Compos. Part A Appl. Sci. Manuf.* **2022**, *161*, 107105. [CrossRef]
35. Michel, S.; Murphy, N.; Kinloch, A.J.; Jones, R. On Cyclic-Fatigue Crack Growth in Carbon-Fibre-Reinforced Epoxy-Polymer Composites. *Polymers* **2024**, *16*, 435. [CrossRef] [PubMed]
36. Clerc, G.; Brunner, A.J.; Niemz, P.; Van De Kuilen, J.W.G. Feasibility study on Hartman-Schijve data analysis for mode II fatigue fracture of adhesively bonded wood joints. *Int. J. Fatigue* **2019**, *221*, 123–140. [CrossRef]
37. Kinloch, A.J.; Jones, R.; Michopoulos, J.G. Fatigue crack growth in epoxy polymer nanocomposites. *Philos. Trans. R. Soc. A* **2021**, *379*, 20200436. Available online: https://royalsocietypublishing.org/doi/full/10.1098/rsta.2020.0436 (accessed on 20 April 2024). [CrossRef] [PubMed]

38. Jones, R.; Peng, P.; Ang, A.S.M.; Aston, R.W.; Schoenborn, N.D.; Phan, N.D. A comparison of the damage tolerance of AA7075-T6, AA2024-T3 and Boeing Space, Intelligence, and Weapons Systems AM built LPBF Scalmalloy. *Aerospace* **2023**, *10*, 733. [CrossRef]
39. Paris, P.C.; Gomez, R.E.; Anderson, W.E. A rational analytic theory of fatigue. *Trend Eng.* **1961**, *13*, 9–14.
40. Irwin, G.R. Fracture Dynamics, in Fracturing of Metals. *Clevel. Ohio Am. Soc. Met.* **1948**, 147–166.
41. Irwin, G.R. *Handbuch der Physik, 6*; Springer: Berlin/Heidelberg, Germany, 1958; pp. 551–590.
42. Paris, P.C.; Erdogan, F. Critical analysis of crack growth propagation laws. *ASME Trans. J. Basic Eng.* **1963**, *85D*, 528–534. [CrossRef]
43. Paris, P.C. A brief history of the crack tip stress intensity factor and its application. *Meccanica* **2014**, *49*, 759–764. [CrossRef]
44. Frost, N.E. The growth of fatigue cracks. In Proceedings of the First International Conference on Fracture, Sendai, Japan, 12–17 September 1965; Yokobori, T., Ed.; The Japanese Society for Strength and Fracture of Materials: Sendai, Japan, 1996; pp. 1433–1459.
45. *ASTM E647-15e1*; Standard Test Method for Measurement of Fatigue Crack Growth Rates. ASTM International: West Conshohocken, PA, USA, 2015.
46. Elber, W. Fatigue crack cyclic closure under cyclic tension. *Eng. Fract. Mech.* **1970**, *2*, 37–45.
47. Elber, W. *ASTM STP 486*; The Significance of Crack Closure. ASTM International: West Conshohocken, PA, USA, 1971; pp. 230–242.
48. Kemp, R.M.J. Fatigue Crack Closure—A review, Royal Aerospace Establishment, Technical Report 90046, Procurement Executive, Ministry of Defence, Farnborough, Hampshire, UK, September 1990. Available online: https://apps.dtic.mil/sti/pdfs/ADA236760.pdf (accessed on 20 April 2024).
49. Paris, P.C.; Tada, H.; Donald, J.K. Service load fatigue damage—A historical perspective. *Int. J. Fatigue* **1999**, *21*, S35–S46. [CrossRef]
50. Paris, P.C.; Lados, D.; Tada, H. Reflections on identifying the real $\Delta K_{effective}$ in the threshold region and beyond. *Eng. Fract. Mech.* **2008**, *75*, 299–305. [CrossRef]
51. Kujawski, D. Enhanced model of partial crack closure for correlation of R-ratio Effects in aluminium alloys. *Int. J. Fatigue* **2001**, *23*, 95–102. [CrossRef]
52. Ribeiro, V.; Correia, J.; Lesiuk, G.; Gonçalves, A.; De Jesus, A.; Berto, F. Application and discussion of various crack closure models to predict fatigue crack growth in 6061-T651 aluminium alloy. *Int. J. Fatigue* **2021**, *153*, 106472. [CrossRef]
53. Schijve, J. Some formulas for the crack opening stress level. *Engng Fract. Mech.* **1981**, *14*, 461–465. [CrossRef]
54. Zhang, S.; Marissen, R.; Schulte, K.; Trautmann, K.K.; Nowack, H.; Schijve, J. Crack propagation studies on Al7475 on the basis of constant amplitude and selective variable amplitude loading histories. *Fatigue Engrg. Mater.Struct.* **1987**, *10*, 315–332. [CrossRef]
55. Kumar, R.; Singh, K. Influence of stress ratio on fatigue crack growth in mild steel. *Eng. Fract. Mech.* **1995**, *50*, 377–384. [CrossRef]
56. Newman, J.C., Jr. A crack opening stress equation for fatigue crack growth. *Int. J. Fatigue* **1984**, *24*, 131–135. [CrossRef]
57. *ASTM STP 748*; A Crack-Closure Model for Predicting Fatigue Crack Growth under Aircraft Spectrum Loading. American Society for Testing and Materials: Philadelphia, PA, USA, 1981; pp. 53–84.
58. Skorupa, M. Load interaction effects during fatigue crack growth under variable amplitude loading—A literature review. Part II: Qualitative interpretation. *Fatigue Fract. Engng. Mater. Struct.* **1998**, *22*, 905–926. [CrossRef]
59. Donald, K.; Paris, P.C. An evaluation of ΔK estimation procedure on 6061-T6 and 2024-T3 aluminum alloys. *Int. J. Fatigue* **1999**, *21*, S47–S57. [CrossRef]
60. Walker, K.F.; Wang, C.H.; Newman, J.C., Jr. Closure measurement and analysis for small cracks from natural discontinuities in an aluminium alloy. *Int. J. Fatigue* **2016**, *82*, 256–262. [CrossRef]
61. Jones, R. Fatigue crack growth and damage tolerance. *Fatigue Fract. Engng. Mater. Struct.* **2014**, *37*, 463–483. [CrossRef]
62. van Kuijk, J.J.A.; Alderliesten, R.C.; Benedictus, R. Unraveling the myth of closure corrections: Sharpening the definition of opening and closure stresses with an energy approach. *Int. J. Fatigue* **2020**, *143*, 106016. [CrossRef]
63. Newman, J.C., Jr.; Edwards, P.R. Short-Crack Growth Behaviour in an Aluminium Alloy—An AGARD Cooperative Test Programme, AGARD-R-732, December 1988. Available online: https://ntrs.nasa.gov/citations/19890007916 (accessed on 1 January 2022).
64. Liu, J.; Chen, J.; Sun, Z.; Zhang, H.; Yuan, Q. A Study on Fatigue Crack Closure Associated with the Growth of Long Crack in a New Titanium Alloy. *Metals* **2023**, *13*, 1377. [CrossRef]
65. Kujawski, D.; Sadananda, K.; Vasudevan, A.K.; Ricker, R.E. On 50 years of fatigue crack closure dispute. *Fatigue Fract. Eng. Mater. Struct.* **2023**, *46*, 2816–2829. [CrossRef]
66. Hartman, A.; Schijve, J. The effects of environment and load frequency on the crack propagation law for macro fatigue crack growth in aluminum alloys. *Eng. Fract. Mech.* **1970**, *1*, 615–631. [CrossRef]
67. Endo, M.; McEvily, A.J. Prediction of the behaviour of small fatigue cracks. *Mater. Sci. Eng A* **2007**, *468–470*, 51–58. [CrossRef]
68. Ishihara, S.; McEvily, A.J. Analysis of short fatigue crack growth in cast aluminium alloy. *Int. J. Fatigue* **2002**, *24*, 1169–1174. [CrossRef]
69. Zheng, X.; Hirt, M. Fatigue crack propagation in steels. *Eng. Fract. Mech.* **1983**, *18*, 965–973.
70. Maierhofer, J.; Pippan, R.; Gänser, H.P. Modified NASGRO equation for physically short cracks. *Int. J. Fatigue* **2014**, *59*, 200–207. [CrossRef]
71. Pourheidar, A.; Patriarca, L.; Beretta, S.; Regazzi, D. Investigation of Fatigue Crack Growth in Full-Scale Railway Axles Subjected to Service Load Spectra: Experiments and Predictive Models. *Metals* **2021**, *11*, 1427. [CrossRef]

72. Davidson, D.L.; Lankford, J. Fatigue crack growth mechanics for Ti-6AI-4V (RA) in vacuum and humid air. *Metall. Trans. A* **1984**, *15A*, 1931–1940. [CrossRef]

73. Davidson, D.L.; Langford, J. Fatigue crack growth in metals and alloys: Mechanisms and micromechanics. *Int. Mater. Rev.* **1992**, *37*, 45–76. [CrossRef]

74. Liu, H.W.; Liu, D. A quantitative analysis of structure sensitive fatigue crack growth in steels. *Scr. Metall.* **1984**, *18*, 7–12. [CrossRef]

75. Chapetti, M.D. Fatigue propagation threshold of short cracks under constant amplitude loading. *Int. J. Fatigue* **2003**, *25*, 1319–1326. [CrossRef]

76. Wang, H.; Wang, F.; Cui, W.; Hayat, T.; Ahmad, B. Prediction of short fatigue crack growth of Ti-6Al-4V. *Fatigue Fract. Eng. Mater. Struct.* **2014**, *37*, 1075–1086. [CrossRef]

77. Božić, Z.; Mlikota, M.; Schmauder, S. Application of the ΔK ΔJ and ΔCTOD Parameters in Fatigue Crack Growth Modelling, Technical Gazette 2011; pp. 3459–3466, ISSN 1330-3651. Available online: https://hrcak.srce.hr/71828 (accessed on 19 April 2024).

78. Masuda, K.; Oguma, N.; Ishihara, S.; McEvily, A.J. Investigation of subsurface fatigue crack growth behavior of D2 tool steel (JISSKD11) based on a novel measurement method. *Int. J. Fatigue* **2020**, *133*, 105395. [CrossRef]

79. McEvily, A.J.; Ishihara, S. On the dependence of the rate of fatigue crack growth on the σ^n_a (2a) parameter. *Int. J. Fatigue* **2001**, *23*, 115–120. [CrossRef]

80. McEvily, A.J.; Eifler, D.; Macherauch, E. An analysis of the growth of short fatigue cracks. *Eng. Fract. Mech.* **1991**, *40*, 571–584. [CrossRef]

81. Jones, R.; Peng, D.; Sing Raman, R.K.; Kinloch, A.J.; Michopoulos, J. Thoughts on two approaches for accounting for the scatter in fatigue delamination growth curves. *Compos. Struct.* **2021**, *258*, 113175. [CrossRef]

82. Main, B.; Jones, M.; Dixon, B.; Barter, S. On small fatigue crack growth rates in AA7085-T7452. *Int. J. Fatigue* **2022**, *156*, 106704. [CrossRef]

83. He, J.; Liu, Y.; Liu, C.; Wang, Q.; Ma, L. Fatigue Crack Growth Rate of an Al-Cu-Mg Alloy. *IOP Conf. Ser. Earth Environ. Sci.* **2019**, *237*, 032122. [CrossRef]

84. da Fonte, M.; Romeiro, F.; de Freitas, M.; Stanzl-Tschegg, S.E.; Tschegg, E.K.; Vasudevan, A.K. The effect of microstructure and environment on fatigue crack growth in 7049 aluminium alloy at negative stress ratios. *Int. J. Fatigue* **2003**, *25*, 1209–1216. [CrossRef]

85. Smith, S.W.; Piascik, R.S. Fatigue Crack Growth Characteristics of Thin Sheet Titanium Alloy Ti6-2-2-2-2, NASA Technical Memorandum NASA/TM-2001-210830, March 2001. Available online: https://ntrs.nasa.gov/citations/20010032404 (accessed on 20 April 2024).

86. Liu, H.; Yang, X.; Li, S.; Yan, C.; Huan, J. Influence of temperature on the R-effect for the fatigue crack growth of nickel-base superalloy GH4169. *Fatigue Fract. Eng. Mater. Struct.* **2022**, *45*, 3025–3039. [CrossRef]

87. Karapuzha, A.S.; Wegener, T.; Krochmal, M.; Zhu, Y.; Niendorf, T.; Fraser, D.; Wu, X.; Huang, A. Fatigue crack growth in additively manufactured Hastelloy X—Influences of crack orientation and post-fabrication treatments. *Mater. Sci. Eng. A* **2022**, *854*, 143773. [CrossRef]

88. Hu, X.; Xue, Z.; Ren, T.; Jiang, Y.; Dong, C.; Liu, F. On the fatigue crack growth behaviour of selective laser melting fabricated Inconel 625: Effects of build orientation and stress ratio. *Fatigue Fract. Eng. Mater. Struct.* **2020**, *43*, 771–787. [CrossRef]

89. Mei, Z.; Morris, J.W. Influence of Deformation-Induced Martensite on Fatigue Crack Propagation in 304-Type Steels. *Metall. Trans.* **1990**, *21A*, 3137–3153. [CrossRef]

90. Rackwitz, J.; Yu, Q.; Yang, Y.; Laplanche, G.; George, E.P.; Minor, A.M.; Ritchie, R.O. Effects of cryogenic temperature and grain size on fatigue-crack propagation in the medium-entropy CrCoNi alloy. *Acta Mater.* **2020**, *200*, 351–365. [CrossRef]

91. Forth, S.C. The Purpose of Generating Fatigue Crack Growth Threshold Data, NASA Johnson Space Center. 2009. Available online: http://ntrs.nasa.gov/ (accessed on 20 April 2024).

92. Forth, S.C.; Johnston, W.M.; Seshadri, B.R. The effect of the laboratory specimen on fatigue crack growth rate. Fracture of Nano and Engineering Materials and, Structures, Alexandropoulos, Greece, 7 July 2006; Gdoutos, E.E., Ed.; Springer: Dordrecht, The Netherlands; pp. 457–458, ISBN 978-1-4020-4971-2. [CrossRef]

93. Newman, J.C., Jr.; Ruschau, J.J.; Hill, M.R. Improved test method for very low fatigue-crack-growth-rate data. *Fatigue Fract. Eng. Mater. Struct.* **2011**, *34*, 270–279. [CrossRef]

94. Newman, J.C., Jr. Analyses of Fatigue Crack Growth Databases for Use in a Damage Tolerance Approach for Aircraft Propellers and Rotorcraft, DOT/FAA/AR-07/49, November 2007. Available online: https://www.tc.faa.gov/its/worldpac/techrpt/ar0749.pdf (accessed on 20 April 2024).

95. Forth, S.C.; James, M.A.; Johnston, W.M.; Newman, J.C., Jr. Anomalous fatigue crack growth phenomena in high-strength steel. In Proceedings of the International Congress on Fracture, Torino, Italy, 20–25 March 2005. Available online: https://ntrs.nasa.gov/citations/20050158690 (accessed on 1 May 2023).

96. Pokorny, P.; Vojtek, T.; Náhlík, L.; Hutar, P. Crack closure in near-threshold fatigue crack propagation in railway axle steel EA4T. *Eng. Fract. Mech.* **2017**, *185*, 2–19. [CrossRef]

97. Henaff, G.; Petit, J.; Bouchet, B. Environmental influence on the near-threshold fatigue crack propagation behaviour of a high strength steel. *Int. J. Fatigue* **1992**, *14*, 211–218. [CrossRef]

98. Wanhill, R.; Barter, S.; Molent, L. *Fatigue Crack Growth Failure and Lifing Analyses for Metallic Aircraft*; Springer Briefs in Applied Sciences and Technology; Springer: Berlin/Heidelberg, Germany, 2019; ISBN 978-94-024-1673-2. [CrossRef]

99. Schijve, J. Fatigue of structures and materials in the 20th century and the state of the art. *Int. J. Fatigue* **2003**, *25*, 679–702. [CrossRef]

100. Schönbauer, B.M.; Stanzl-Tschegg, S.E.; Perlega, A.; Salzman, R.N.; Rieger, N.F.; Turnbull, A.; Zhou, S.; Lukaszewicz, M.; Gandy, D. The influence of corrosion pits on the fatigue life of 17-4PH steam turbine blade steel. *Eng. Fract. Mech.* **2015**, *147*, 158–175. [CrossRef]

101. Virkler, D.A.; Hillberry, B.M.; Goel, P.K. The statistical nature of fatigue crack propagation. *Trans. ASME* **1979**, *101*, 148–153. [CrossRef]

102. Oldersma, A.; Wanhill, R.J.H. *Variability of Fatigue Crack Growth Properties for 2024-T3 Aluminium Alloy, NLR TP 96038*; National Aerospace Laboratory NLR: Amsterdam, The Netherlands, 1996.

103. NASA-HDBK-5010; Fracture Control Handbook for Payloads, Experiments, and Similar Hardware, May 2005, Revalidated 2012. Available online: https://standards.nasa.gov/standard/nasa/nasa-hdbk-5010 (accessed on 2 January 2024).